CDF/PLUG_UPGR/DOC/CDFR/2453
TS-DET 94-005
2/7/94
Version 1.0

Proposal to Include a Preshower Detector as Part of the CDF End Plug Upgrade

M. Albrow(2), P. de Barbaro(6), V. Barnes(5), J. Freeman(2), R. Harris(2), J. Huston(4), S. Kim(8), K. Kondo(8), P. Limon(2), M. Lindgren(1), P. Melese(7), M. Mishina(3), S. Miyashita(8), T. Müller(1), Y. Shima(8), J. Strait(2), T. Takebayashi(8)

(1)University of California at Los Angeles, (2)Fermilab, (3)KEK, (4)Michigan State University, (5)Purdue University, (6)University of Rochester, (7)Rockefeller University, (8)University of Tsukuba

Contents

1 Introduction

We propose to build a preshower detector which will be part of the plug upgrade electromagnetic calorimeter. Figure 1 shows a cross-section of one-quarter of the CDF central detector with the upgrade end plugs showing the segmentation in pseudorapidity, and Figure 2 shows the transverse segment of one 15° slice of the Plug Upgrade EM calorimeter (PEM). The parameters of the PEM with the proposed Plug PReshower detector (PPR) are summarized in Table 1. The EM calorimeter covers the range η = 1.1 to 3.5 (θ = 37° to 3.5°). It is divided into projective towers with $\Delta\eta$ x $\Delta\phi \cong$ 0.11 x 0.13 at low η but with coarser segmentation at larger η. The preshower detector is at a depth along the z-axis of 1.5 X_0 and has the same transverse segmentation as the rest of the PEM. It is implemented by replacing the first PEM sampling layer with a special scintillator layer which is read out separately. Following the PPR are 22 layers of the EM calorimeter, which has a 0.87 X_0

Table 1: Plug Upgrade EM Calorimeter Parameters

Sampling Thicknesses (in z-direction)		
Calorimeter sampling thickness	0.87 X_0	0.04 λ_I
Pre-radiator (includes CTC end plate, etc.)	1.5 X_0	0.21 λ_I
Shower maximum detector depth	5.0 X_0	0.39 λ_I
Number of samples (including preshower)	23	
z-coordinate of PPR (center of gap)	1773 mm from the IP	

Transverse Segmentation								
							Preshower	
θ_1	θ_2	η_1	η_2	$\Delta\eta$	$\Delta\phi$		Δr(mm)	$r\Delta\phi$(mm)
36.82°	33.52°	1.10	1.20	0.10	0.13	(7.5°)	155	163
33.52°	30.00°	1.20	1.32	0.12	0.13	(7.5°)	150	143
30.00°	27.30°	1.32	1.42	0.10	0.13	(7.5°)	108	126
27.30°	24.60°	1.42	1.52	0.11	0.13	(7.5°)	103	113
24.60°	21.90°	1.52	1.64	0.12	0.13	(7.5°)	99	99
21.90°	19.20°	1.64	1.78	0.13	0.13	(7.5°)	95	87
19.20°	16.50°	1.78	1.93	0.15	0.13	(7.5°)	92	74
16.50°	13.80°	1.93	2.11	0.18	0.13	(7.5°)	89	63
13.80°	11.10°	2.11	2.33	0.22	0.26	(15°)	87	102
11.10°	8.40°	2.33	2.61	0.28	0.26	(15°)	86	79
8.40°	5.70°	2.61	3.00	0.39	0.26	(15°)	84	57
5.70°	3.46°	3.00	3.50	0.52	0.26	(15°)	71	37

sampling thickness. There is a shower maximum position detector (SMD) after 4 EM sampling layers (plus the PPR) at a z-projected depth of 5 X_0. It consists of 5 mm wide

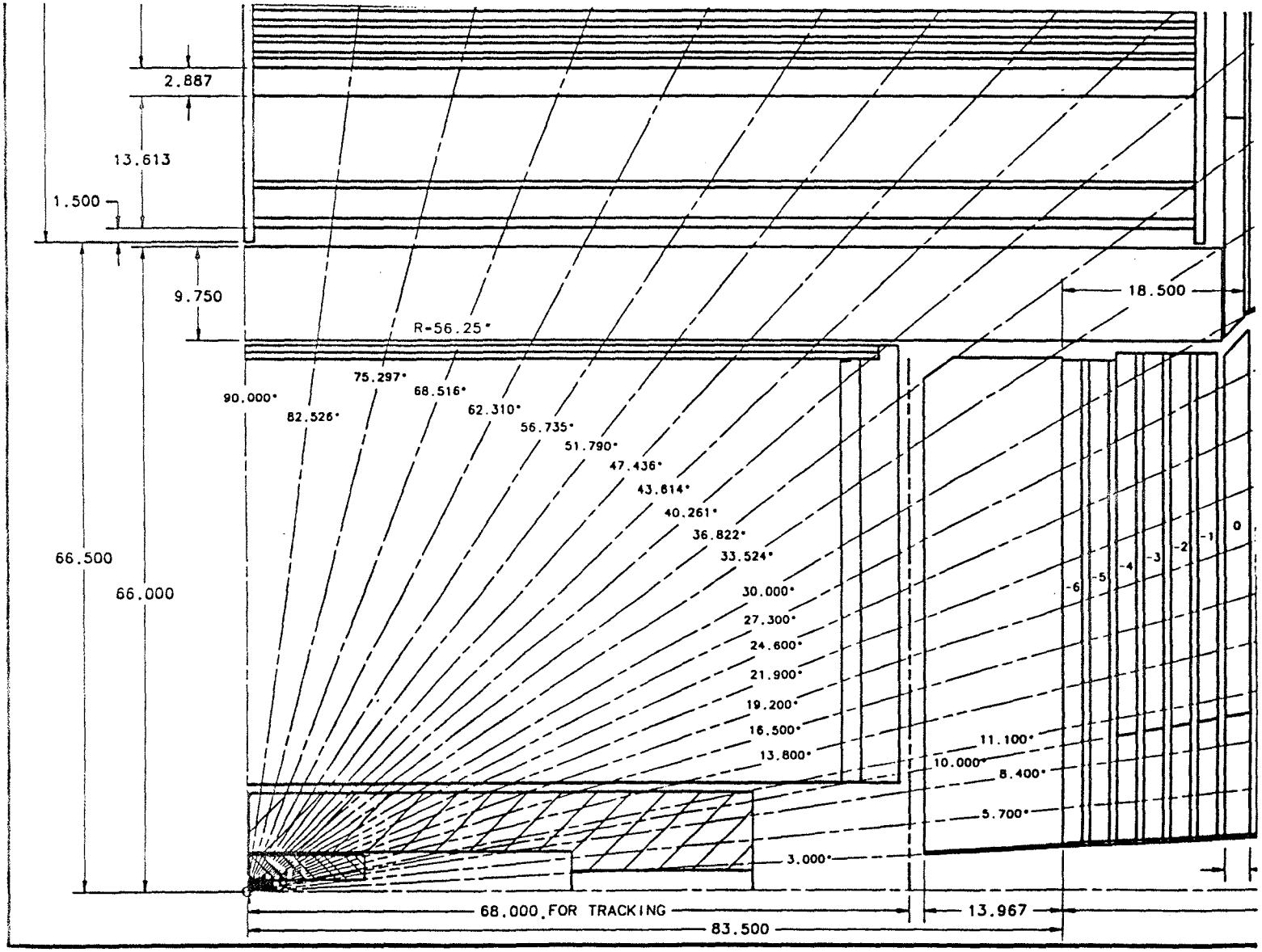

Figure 1: Cross-section of one-quarter of the CDF central detector with the end plug upgrade. The dashed lines radiating from the interaction point indicate the η segmentation of the calorimeters.

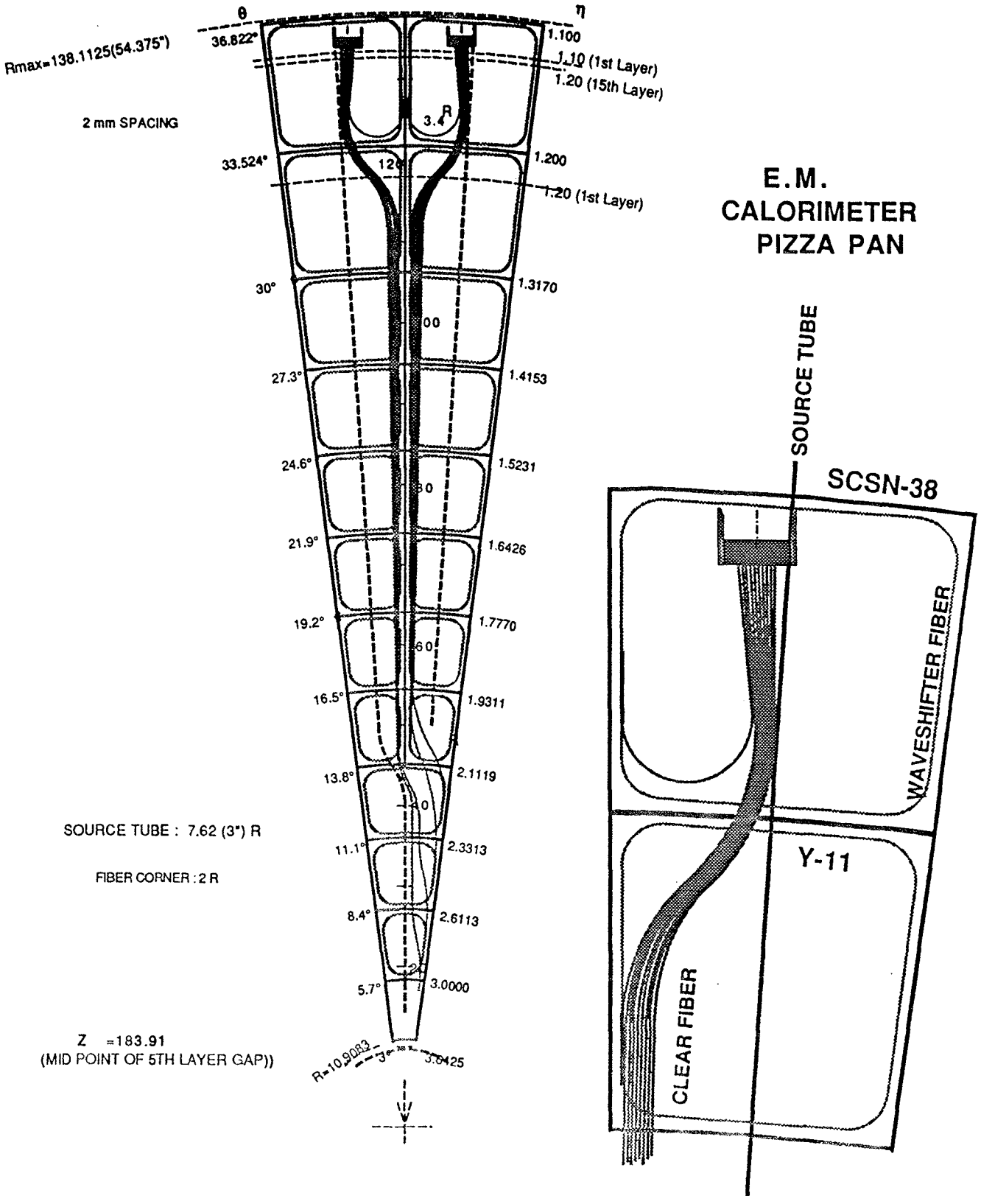

Figure 2: Plug Upgrade EM calorimeter scintillator assembly ("pizza pan") showing the transverse segmentation, wavelength shifter and clear fiber routing, and tubes for routing a wire actuated radioactive source for calibration.

scintillating strips in two 45° stereo views, and it is subdivided into two pseudorapidity segments at $\eta = 2.6$.

The preshower detector will be used to enhance the ability to do physics with photons and electrons and is complimentary to the shower maximum position detector. Rejection of charged pions is improved by requiring a large pulse height in the preshower detector. The fraction of single photons in a sample of neutral particles produing electromagnetic showers can be determined due to the higher probability of conversion of the two photons from π^0s than of a single photon. The thickness of the material before the preshower (the preradiator) is chosen to optimize $e^{\pm} - \pi^{\pm}$ and $\gamma - \pi^0$ separation. To be fully efficient for detecting single photon conversions more light is required from the preshower detector than from a standard EM calorimeter sampling layer. Therefore the preshower scintillator will be thicker and of a brighter type than used in the calorimeter. Scintillator readout will be provided by multichannel photomultiplier tubes (MCPMTs) of the same type as for the shower maximum position detector. Including a preshower detector as part of the plug upgrade will require only minor modifications of the EM calorimeter and only a small additional cost. Later implementation would be more difficult.

Section 2 of this Proposal will give the physics motivation for including a preshower detector in the end plugs. Section 3 will discuss the design of the proposed detector, including the choice of thickness of the preradiator, requirements on the amount of light from the scintillator, choice of scintillator type and thickness, the design of the multi-tile scintillator assemblies ("pizza pans"), the MCPMT readout, and mechanical integration with the PEM lead structure. The expected performance of the preshower detector, including how to sum its energy measurement with that from the calorimeter, will be presented in Section 4. Calibration methods will be discussed in Section 5, and a cost estimate and schedule requirements will be presented in Section 6.

2 Physics Motivation

The plug preshower detector will be used for measurements of physics within the Standard Model and beyond. It will be used for QCD direct photon physics, electroweak physics, heavy flavor physics, and exotic particle searches. The preshower detector gives enhanced $\gamma - \pi^0$ and $e - \pi^{\pm}$ separation in the forward region over what would be available without it. The plug preshower will improve the discrimination of charged pions from electrons by a factor 2 or more, and it gives the ability to do single photon physics over the full momentum scale, a capability which does not exist without it.

2.1 Direct Photons

2.1.1 QCD

Thus far, measurements of prompt photons at CDF have been concentrated in the central region[1], at least partially because of the lack of adequate detection tools in the plug region. The plug preshower detector will give us the capability to separate photons from the neutral meson background in the new end plugs over a wide kinematic range. The shower maximum

position detector currently being built for the plug upgrade, will help to distinguish multi-π^0 jets and single π^0's from single photons but only over a limited P_T range.

The primary motivation for measuring prompt photons in hadron collisions is to test QCD and measure the gluon distribution of the proton. The dominant subprocess for prompt photon production is the gluon Compton scattering diagram[2]. Extending photon measurements to the plug would add a great deal to our knowledge of the gluon distribution, and if the measurement can be performed at low P_T, would help to determine the gluon behavior at small x, where it is least well known. These values of x are not accessible from photon measurements in the central region. Jets can also be measured at high values of rapidity but the energy determination of a jet is much more difficult than that of a direct photon, especially at low values of P_T.

The photon rapidity distribution (for P_T in the range of 10 GeV) will show a strong peaking near a rapidity of 3 if the gluon has a singular behavior as x approaches zero. This behavior is shown in Figure 3[2]. A similar peaking will not be seen in jet production due to the dominance of the t-channel gluon exchange pole, absent in direct photon production at lowest order.

The direction of the away-side jet can in addition be measured, and then the kinematics of the hard scatter are completely determined in lowest order QCD. Table 2 shows the smaller and larger x of the two incoming partons as a function of the absolute pseudorapidity of the jet and the parton for a 10 GeV jet taken from the lowest order equation $x_{1,2} = (P_T/\sqrt{s})\,[\exp(\pm\eta_\gamma) + \exp(\pm\eta_{JET})]$. By using the jet opposite the photon we can measure values of x as low as 6×10^{-4}, at least a factor of 6 smaller than if the plug were not used for photon identification. The small x measurements of the gluon distribution are competitive with or exceed those possible at HERA[3]. Also, the PPR allows us to measure values of x twice as high as can be measured with central photons.

$\lvert\eta\rvert$	0.5	1.5	3.0	0.5	1.5	3.0
0.5	.0067	.0046	.0036	.018	.034	.120
1.5	.0046	.0025	.0015	.034	.050	.136
3.0	.0036	.0015	.0006	.120	.136	.223
	Smaller x			Larger x		

Table 2: The smaller and larger value of fractional momentum x in photon + jet events with $P_T = 10$ GeV as a function of the pseudorapidity of the photon and the pseudorapidity of the jet (rows and columns).

QCD measurements using the jet in photon events are performed regularly at CDF. The photon P_T distribution with the jet in a specific pseudorapidity region has been measured[4] and can be improved by using the PPR to extend the sensitivity of the measurement at both low and high x. Using the PPR, the photon plus jet center of mass angular distribution measurement[5] can be extended to higher values of $\cos\theta^*$. Current measurements show a disagreement with NLO QCD predictions at high values of $\cos\theta^*$. Also, using central photons CDF has made the first measurement of the photon + charm cross section, which

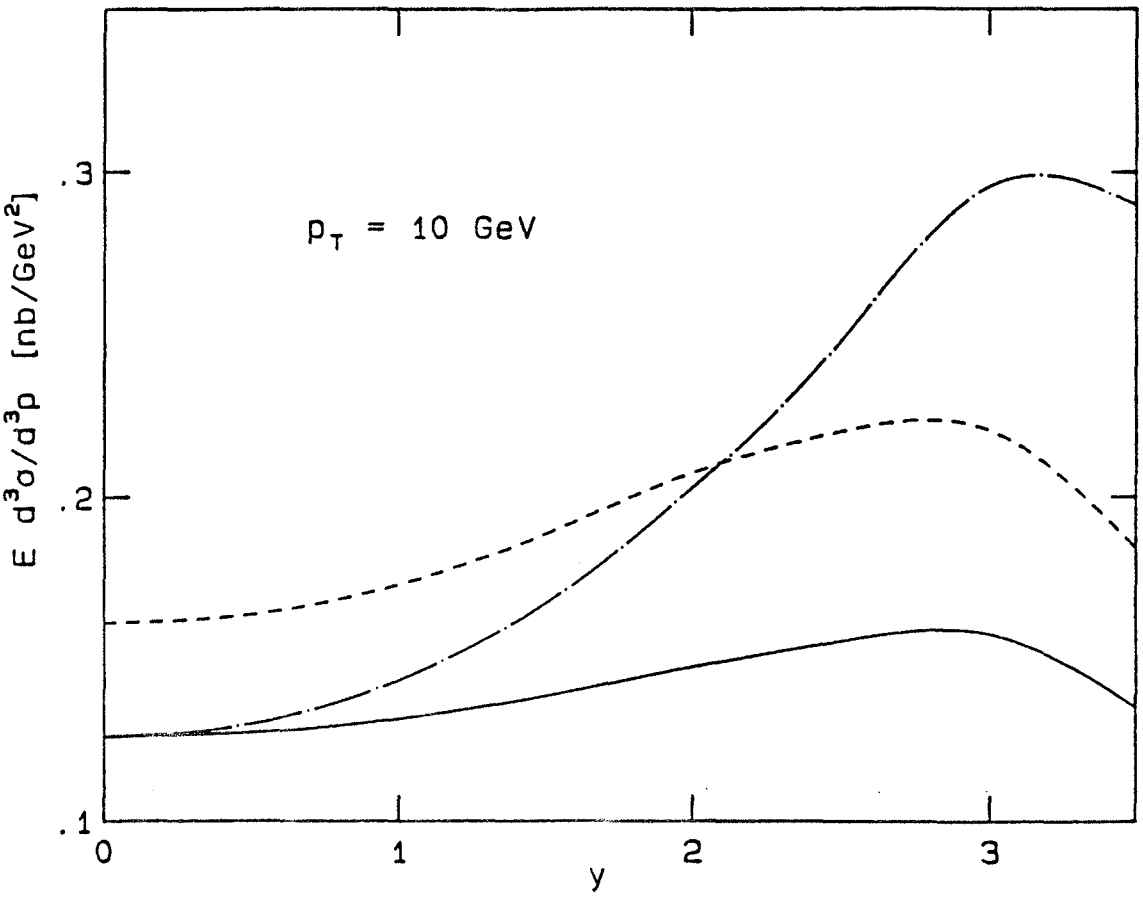

Figure 3: The cross section for prompt photon production vs. rapidity for a photon with 10 GeV P_T is shown for standard parton distributions (solid), a soft gluon distribution (dashed), and a singular gluon distribution (dot dashed).

will allow the first direct measurement of the charm quark distribution of the proton. Here the final state charmed quark is tagged either by a reconstructed D* meson[6] or by its semileptonic decay to a muon[7]. The PPR will both increase the statistics and x range of this unique measurement. Another important test of QCD is the measurement of two prompt photons, a large background to the search for the Higgs boson at future hadron colliders. This measurement is currently limited by low statistics[8] when both photons are confined to the central region alone. Adding the PPR will increase the statistics of two prompt photons by an order of magnitude if the pseudorapidity distribution is flat in η. The PPR will also help the photon plus two jet measurement[9], which also suffers from low statistics.

2.1.2 Other Direct Photon Physics

In addition to QCD, prompt photons are also useful to search for physics beyond the standard model. The PPR will increase the acceptance for these measurement by providing a reliable estimate of the neutral meson backgrounds in the plug region. During the 1989 and 1992-93 runs we found several events with anomalously high diphoton mass and total event transverse energy[10]. The PPR would increase our sensitivity to this possible signal of new physics. Also during the 1992-93 run we used central prompt photons to search for excited states of composite quarks decaying into a quark and a photon[11] ($qg \rightarrow q* \rightarrow q\gamma$). The PPR could contribute to higher limits on excited quark mass in this channel. In the 1989 and 1992 runs we measured the cross section for $W + \gamma$ production[12] and $Z + \gamma$ production. In addition to being an interesting measurement of electroweak predictions for the trilinear coupling of gauge bosons, the measurement probes the anomalous magnetic moment that would occur if the W and Z were composite particles. The PPR will allow for higher statistics measurements of the trilinear coupling and a more significant limit on W and Z compositeness.

2.2 Electrons

In addition to photon physics the PPR can be used to improve the ability of CDF to do physics involving electrons. Good electron identification over as large a pseudorapidity range as possible is particularly important for heavy flavor physics. The PPR can be used to improve the event-by-event rejection of charged pions by more than a factor of 2. Analysis of the pulse height distribution from the PPR can also be used to determine statistically the electron fraction in a sample of electron candidates, a method which has been used with the CPR[13]. Because momentum resolution in the plug region is at best poor, the additional information from a preshower detector may be relatively more important in the plug than in the central region for identifying electrons and for understanding the systematic errors in the electron - pion separation algorithms.

To search for or study the properties of the top quark, the PPR will be used to identify soft leptons as a tag of bottom quarks resulting from top quark decays. The Central Preshower (CPR) has already been used successfully to reduce backgrounds to the top search in the soft lepton tag analysis[14], hence the PPR can increase our acceptance for discovering the top quark and measuring its mass. Inclusion of the plug region in the analysis would increase the acceptance for top events by a factor of 2 or more.

The production of bottom quarks, ocurring predominantly via gluon fusion, is both an important test of next-to-leading order QCD and another measurement of the gluon distribution at low x. The additional η coverage provided by the PPR will both increase the statistics on the current measurement and allow a measurement as a function of η, which will increase the x range by roughly the same amount as it does for prompt photons. Measurement of the bottom quark production cross section using semileptonic decay electrons ($B \rightarrow eX$) is difficult due to large backgrounds from charged pions faking electrons. As a consequence, our first measurement[15] was too high by roughly 1 σ on its systematic uncertainty, and this error was discovered in part by improved pion rejection using the CPR[13]. The CPR has reduced the considerable systematic uncertainties on the b quark cross section, and we expect that the PPR will play the same essential role.

The $B^0\bar{B}^0$ mixing parameter χ, which can provide constraints on the elements of the CKM matrix, has been measured by CDF[16] using central electrons. In the dielectron mode, the plug's η range could increase the statistics of this measurement by nearly an order of magnitude, and the PPR will reduce the systematic uncertainties on the measurement of plug electrons. Similarly, the PPR will help the measurement of $b\bar{b}$ correlations using $e\mu$ events[17], which is currently done only in the central. Another interesting measurement that can be attempted using the CPR and PPR is identification of the electron in the decay $B \rightarrow D^* e\nu$, which could allow a model independent extraction of the matrix element $|V_{cb}|$[18]. Since electrons from B decay are dominantly at low transverse momentum, where e/π separation is more difficult than at high P_T, it is important to incorporate all the tools possible into the new plugs to maximize out ability to do this important physics.

Since the CPR has already demonstrated its usefulness for top and bottom quark physics, we assume the CPR and PPR will eventually be useful in all such measurements at CDF. One of the advantages of the CDF detector over the D0 detector is its many handles on the position and development of central EM showers using the CPR and the Central Electron Strip chambers (CES). We anticipate that the PPR in conjunction with the SMD will lead to similar benefits. Perhaps the most significant discoveries we will make with the PPR are those we cannot at this moment anticipate.

3 Preshower Detector Design

3.1 Preradiator

The preradiator thickness is chosen to optimize the determination of the γ fraction in a sample of neutral particles and the separation of electrons from charged pions. We consider each in turn.

3.1.1 Requirements for $\gamma - \pi^0$ Separation

The probability that a photon does not convert after passing through a preradiator of thickness x (measured in units of radiation lengths X_0) is

$$P_\gamma = exp(-7x/9).$$

The probability that neither photon from a π^0 (or η) converts is

$$P_{\pi^0} = P_\gamma^2 = exp(-14x/9).$$

In a sample of showers consisting of a fraction f of photons and $(1-f)$ of π^0s the observed fraction of non-conversions has a mean value

$$P_o = fP_\gamma^2 + (1-f)P_{\pi^0}.$$

Therefore, if the observed fraction of showers that do not convert in the preshower detector is P_o, then the best estimate of the fraction of photons in the sample is

$$f_0 = (P_o - P_{\pi^0})/(P_\gamma - P_{\pi^0}). \quad (1)$$

The non-conversion probabilities P_γ and P_{π^0} and their difference $\Delta P = (P_\gamma - P_{\pi^0})$ are plotted as a function of preradiator thickness in Figure 4. The maximum difference is 0.25 at a thickness of 0.9 X_0. However, this depth does not give the smallest statistical error in the estimate of the photon fraction. Assuming that the material thickness and hence the values of P_γ and P_{π^0} are perfectly known, the only source of uncertainty is the statistical fluctuation in the observed non-conversion fraction, which follows binomial statistics. The statistical uncertainty in the value of f is

$$\sigma(f) = \sigma(P_o)/(P_\gamma - P_{\pi^0}).$$

Above 0.9 X_0, both $\sigma(P_o)$ and $(P_\gamma - P_{\pi^0})$ decrease with increasing preradiator thickness. Since the rate of decrease of $\sigma(P_o)$ depends on the value of P_o, the thickness which minimizes $\sigma(f)$ depends on P_o and therefore on the single photon fraction. Figure 5 shows how the uncertainty $\sigma(f)$ varies with preradiator thickness for several assumed photon fractions. The optimal thickness is 2.2 X_0 for 10% photons, and 1.3 X_0 for 50% photons. The optimum is rather broad, however; for example, the value of $\sigma(f)$ is within 10% of the minimum in the range $0.7 < x < 2.1\ X_0$ for a sample of 50% photons and $1.2 < x < 3.2\ X_0$ for 10% photons. So any value between about 1.2 and 2 X_0 is acceptable. Since higher photon fraction samples have a narrower minimum and favor thinner preradiators, a thinner preradiator is weakly favored.

3.1.2 Requirements for $e - \pi^\pm$ Separation

The preshower detector can also help to distinguish between electrons and charged pions, and it can offer additional pion rejection after cuts have been made on the energy in the hadron (PHA) and electromagnetic (PEM) calorimeters and on the energy and transverse shower profile in the shower maximum detector (SMD). A pion which passes electron selection cuts based on PHA, PEM and SMD energy is one which interacts before the SMD in such a way that most of its energy goes into π^0s. A cut requiring large preshower pulse height will reject pions which interact between the PPR and SMD. Thus the farther forward the PPR is placed the larger the potential for rejecting pions. On the other hand, to be efficient for accepting electrons the preshower must be placed at a great enough depth that the electron shower has developed enough to be cleanly distinguished from a minimum ionizing

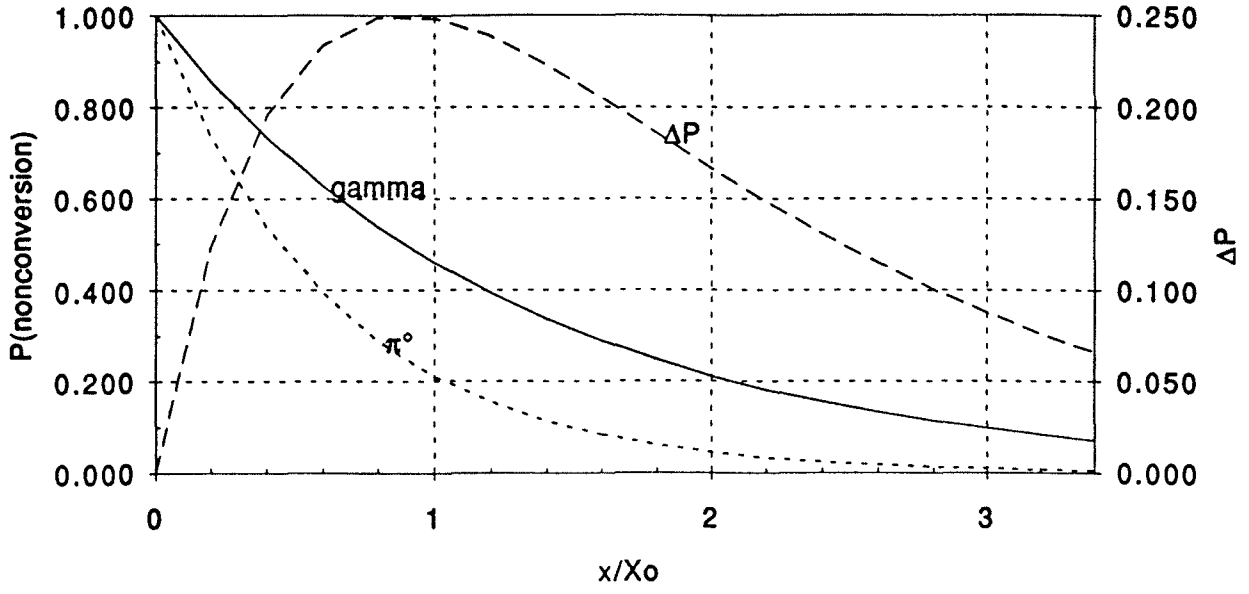

Figure 4: Nonconversion probability versus preshower depth for single photons and π^0s. The difference ΔP between the two probabilities is plotted against the right axis.

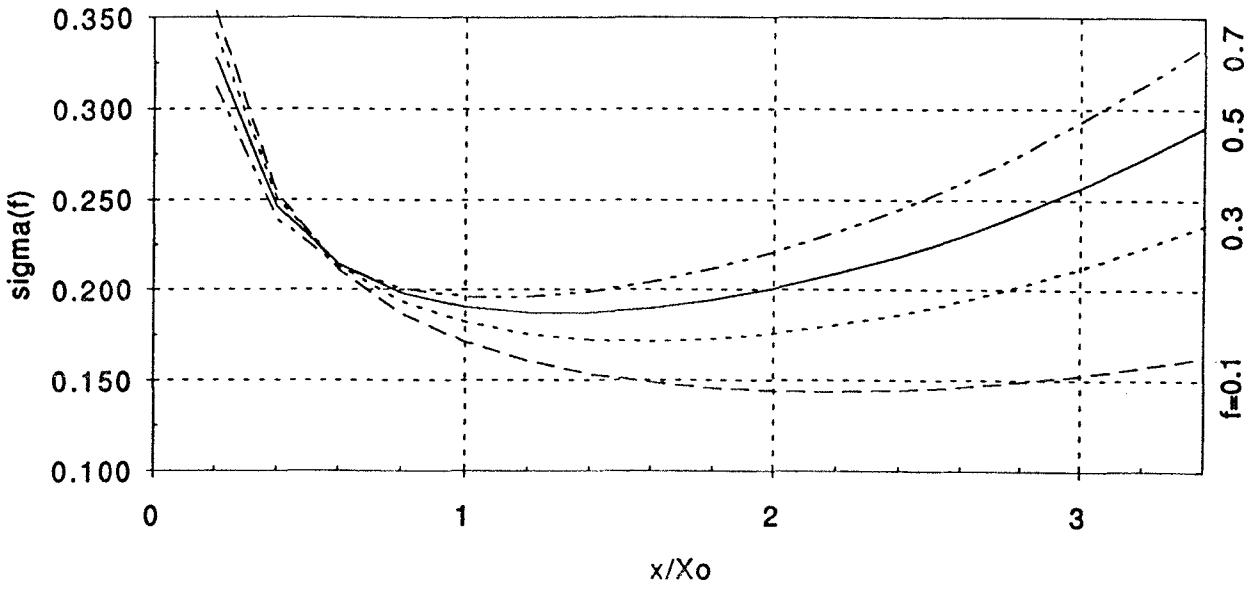

Figure 5: The statistical uncertainty in determining the single photon fraction f in a sample of 100 neutral showers as a function of preshower depth. The different curves correspond to different single photon fractions.

particle. Figure 6 (Figure 11 from[19]) compares the mean energy deposited by electrons and pions as a function of depth as measured in an SDC beam test. As the preradiator thickness increases from 1.0 to 1.75 X_0 the mean energy deposited increases from about 6.4 to 16.6 mips for 10 GeV electrons. Most pions deposit only minimum ionization, but the small fraction of interacting pions gives a mean energy deposition which varies from 1.4 to 2.6 mips as the preradiator thickness increases. Figure 7 (Figure 9 from[19]) presents pulse height distributions from the same SDC beam test for 10 GeV electrons at various depths from 0 to 1.75 X_0. The electron signal is well separated from the mip signal, which corresponds to the electron pulse height for a zero thickness preradiator in Figure 7, for preradiator thickness greater than about 1.5 X_0. Similar results were obtained in a test beam study of the CPR[20] in which the mean electron pulse height increased by almost a factor of 2 as the preradiator thickness increased from 1.1 to 2.0 X_0, but the pion pulse height increased very little. Therefore a preradiator of 1.5 - 2.0 X_0 appears to be a good choice for $e - \pi^{\pm}$ separation.

3.1.3 Choice of Preradiator Thickness

A preradiator thickness of about 1.5 X_0 is a reasonable compromise that satisfies the requirements for $\gamma - \pi^0$ and $e - \pi^{\pm}$ separation. The material between the tracking chambers and the end plug must be considered in computing the effective preradiator thickness. (See Figures 1 and 8.)

The major component of this upstream material is the CTC end plate plus the cables, etc. which lie between it and the plug. The thickness of this material was measured[21] (for the configuration of the '88-'89 run) by comparing the longitudinal shower profiles in the test beam with those from good electrons from W decay. The measured thickness in the z-direction is $x_{CTC} = (0.71 \pm 0.03)\ X_0$. The stainless steel front plate of the plug is $x_{SS} = 6.35$ mm $= 0.36\ X_0$ thick. The pseudorapidity range in the end plug that is usable for single photon and electron measurements is $\eta = 1.1$ to $\eta = 3.0$. (The smallest angle tower, covering $\eta = 3.0$ to $\eta = 3.5$ will be used to define isolation or to provide containment information about particles or jets in the adjacent tower.) At $\eta = 2.0$, roughly in the middle of the plug, $cos\theta = 0.96$. Therefore, we want the sum of the material upstream of the plug plus the material in the plug before the preradiator to be

$$(x_{CTC} + x_{SS} + x_{PPR})/0.96 = 1.5X_0.$$

Therefore we require an explicit preradiator of thickness $x_{PPR} = 0.37\ X_0$ corresponding to 2.0 mm of lead. This is the configuration shown as (b) in Figure 9, which is a plot of the depth in units of X_0 and λ_I for several PEM components. The CTC end plate extends down to about 9.8° from the beam ($\eta = 2.46$). At smaller angles additional material ($\sim$4 mm of lead) will have to be added to the front of the stainless steel front plate to maintain the same thickness. With a preradiator of this thickness, the projected thickness varies from 1.47 X_0 at $\eta = 3.0$ to 1.82 X_0 at $\eta = 1.1$.

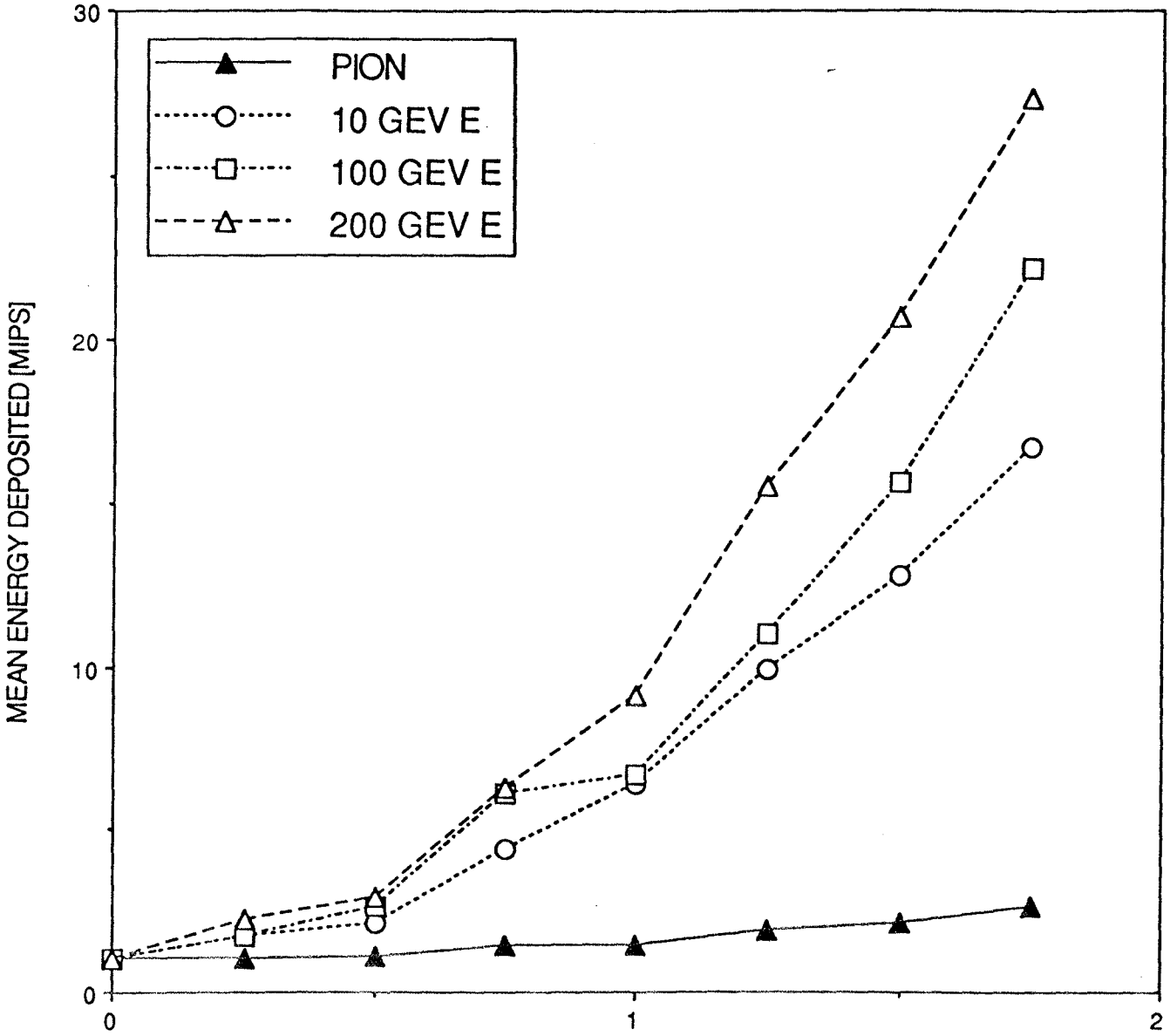

Figure 6: Mean energy deposited, in units of minimum ionizing particles (mips) versus preradiator thickness in radiation lengths for electrons and charged pions in an SDC beam test[19].

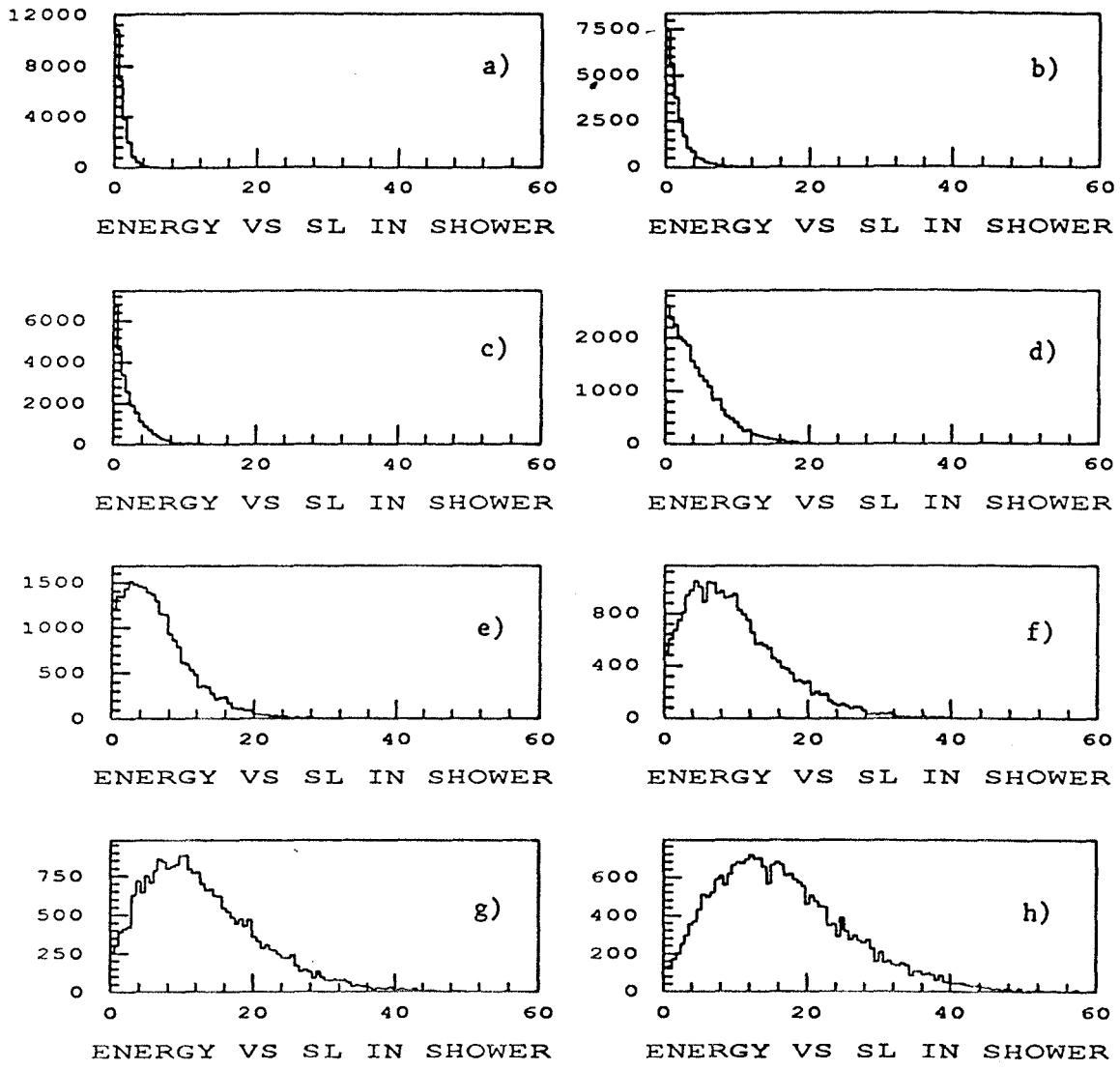

Figure 7: Distribution of energy deposition by 10 GeV electrons (in units of minimum ionizing particles) as a function of the preradiator thickness. Histograms (a) through (h) correspond to preradiator thicknesses of 0 through 1.75 X_0 in steps of 0.25 X_0.

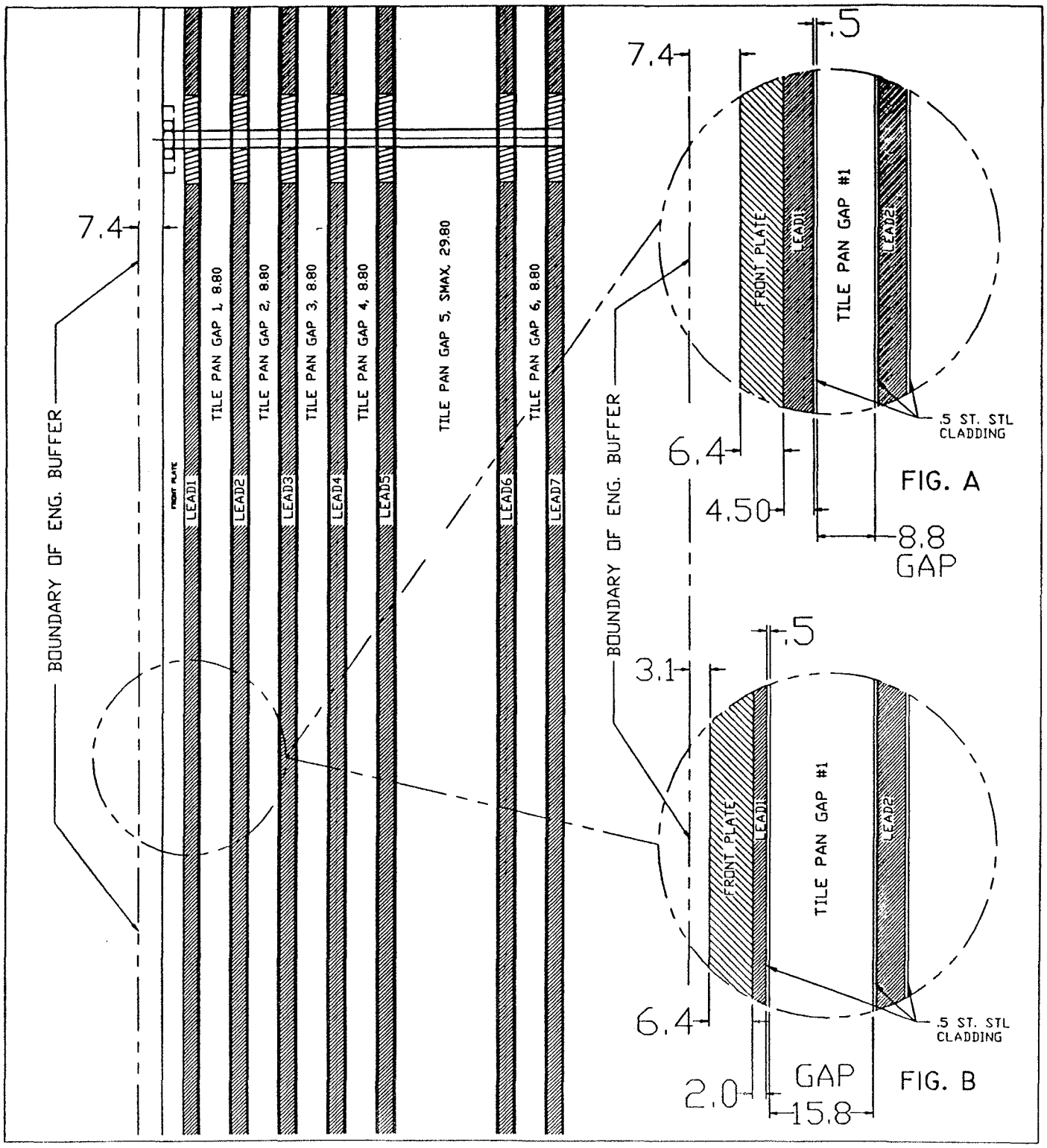

Figure 8: Detail of the longitudinal segmentation of the Plug Upgrade EM calorimeter (PEM) absorbers in the current baseline design (a) and with the proposed preshower detector (b).

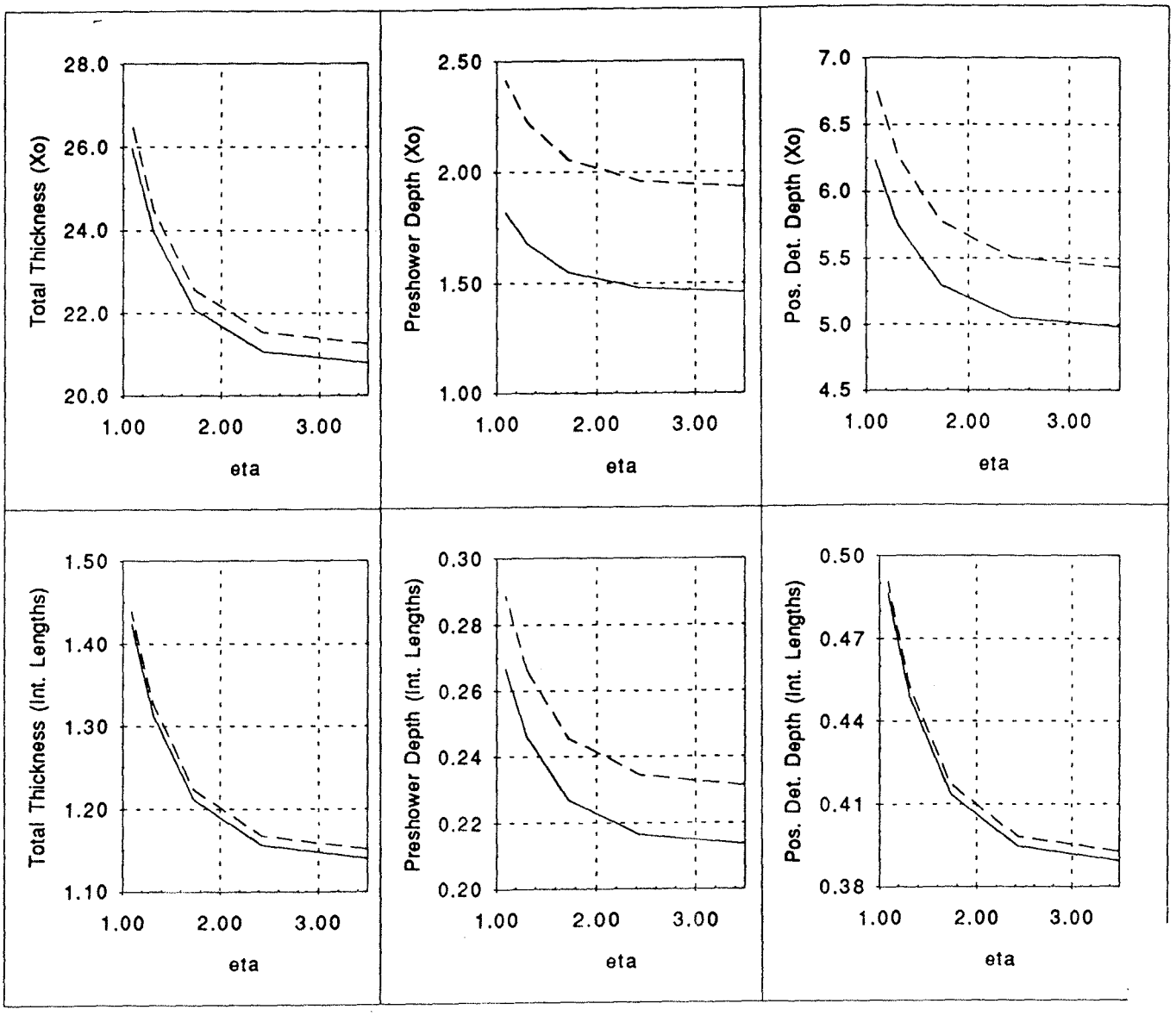

Figure 9: Depth in radiation lengths and interaction lengths of the preshower detector, shower maximum position detector, and the total EM calorimeter for the current plug upgrade design (dashed lines) and the proposed design with a preshower detector (solid lines).

3.2 Scintillator Layer Design

3.2.1 Required Light from the Scintillator

The preshower detector will substitute for the first layer of the electromagnetic calorimeter and will consist of a tile-fiber array with the same segmentation as the rest of the calorimeter. (See Table 1.) The most stringent requirements on the preshower are for $\gamma - \pi^0$ separation. For efficient $\gamma - \pi^0$ separation the preshower detector must be fully efficient for photon conversions, which generate at least 2 minimum ionizing particles (mips), and the photon signal must be cleanly separated from electronic and phototube noise signals. This requires more light than is obtained from a standard EM scintillator layer. Therefore the preshower layer must be made of thicker, brighter scintillator and use more than one turn of wavelength shifter fiber laid in the groove in the scintillator.

The preshower detector will be read out by MCPMTs of the same type as used for the shower maximum detector. In determining how much light is required from the scintillator, the behavior of the MCPMT, including effective quantum efficiency and pulse height resolution, must also be considered. If the photon conversion probability is measured from the data using a sample of π^0s and ηs identified with the shower maximum detector, as has been done in the central region[4, 22], then an inefficiency for detecting a photon conversion of <1% and a noise occupancy (probability that a signal is observed in the absence of a photon conversion) of <0.3% will result in a systematic error of <0.3% in determining the γ fraction in a neutral shower sample[24]. Based on gain and dark current data from two Hamamatsu R5064 MCPMTs, which are the best current candidate tubes for the preshower, and using a Monte Carlo program which simulates the behavior of fine-mesh dynode PMTs[23], it has been shown[24] that 5 photoelectrons per minimum ionizing particle (pe/mip) is sufficient to achieve >99% efficiency with <0.3% PMT noise occupancy.

This is a quite conservative estimate for two reasons. First, the efficiency calculations in[24] assume that a photon conversion always gives exactly two minimum ionizing particles in the preshower detector. In fact, if a photon converts in the preradiator, in most cases a significant shower has developed before the preshower detector layer. For example, Figure 10[25] shows the number of minimum ionizing particles for a sample of 50 GeV (p_T = 13 GeV/c at η = 2) EGS photon showers after a 1.5 X_0 preradiator. For cases in which the photon converts ($N_{mip} > 0$) the mean number of mips is 11 and 83% have > 2 mips. Second, the requirements on efficiency and noise occupancy were chosen to give a systematic error on the determination of the photon fraction from these causes of much less than 1%, while typical systematic errors from other causes are likely to be substantially greater[4, 22]. Further, the statistical error will be also be substantially larger than 1% for isolated neutral particle samples of fewer than 10^4 events. Therefore, in reality a somewhat smaller number of pe/mip could be tolerated without substantially compromising the measurement of photon fractions.

3.2.2 Scintillator - Fiber Configuration Giving the Required Light Output

The light required from the preshower detector (>5 pe/mip) is comparable to that which has been measured for a standard EM calorimeter tile (~5 pe/mip)[26]. However, the effective quantum efficiency (quantum efficiency times collection efficiency) of current multichannel PMTs is only about half that of conventional PMTs with green-extended

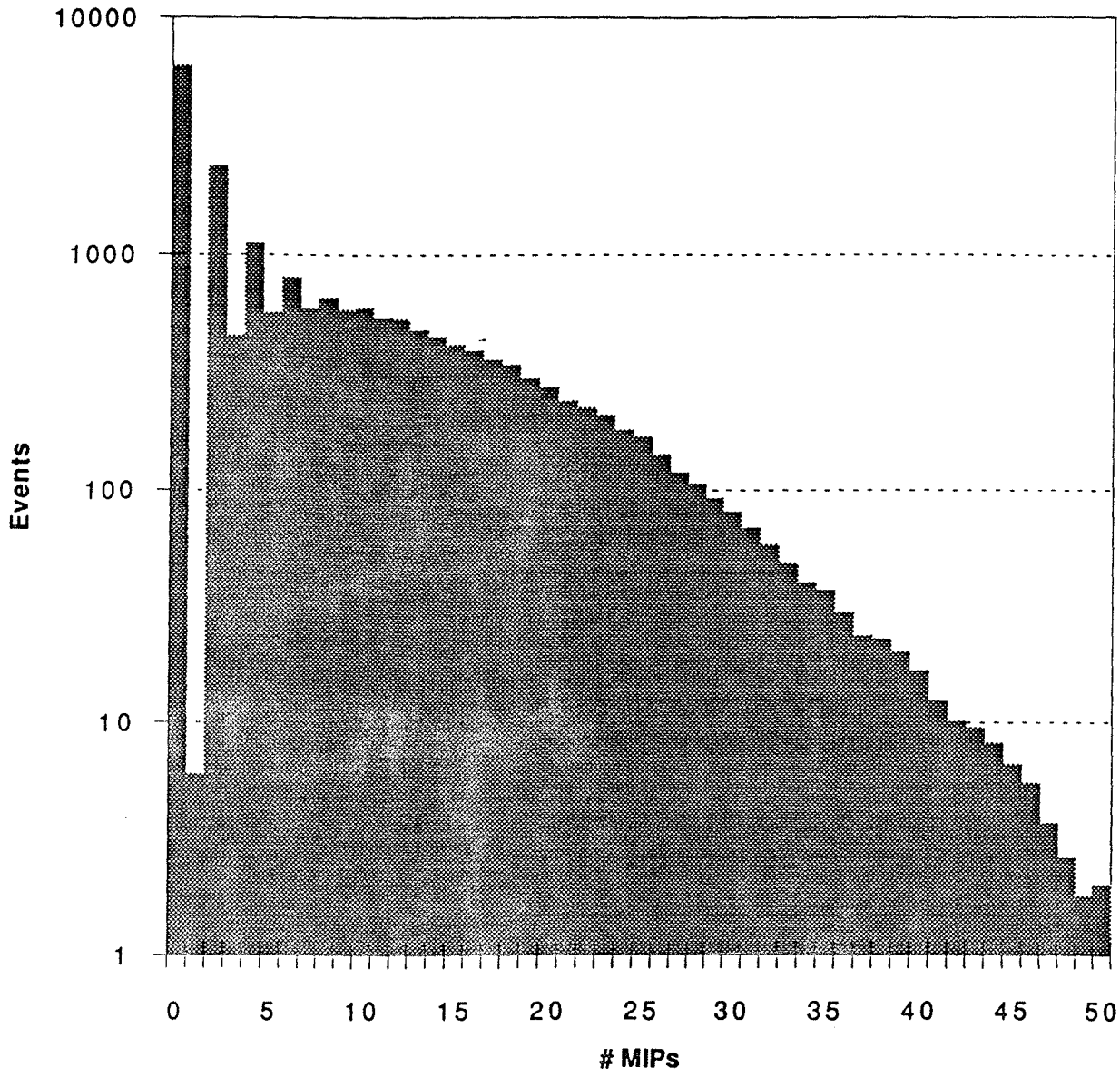

Figure 10: Number of minimum ionizing particles (mips) after a preradiator of thickness 1.5 X_0 for 50 GeV photons from a GEANT simulation[25].

photocathodes[27]. Therefore, brighter, thicker scintillator with more turns of wavelength shifter fiber must be used. Since the space for the preshower is limited (see Section 3.4) there is a premium on using the brightest practical scintillator - fiber combination. Bicron BC408 and BC404 have respectively 30% and 40% greater light output[28] than than Kuraray SCSN38 which is used for the EM and hadron calorimeters, and are therefore favored. Additional light can be obtained by putting two rather than one turn of wavelength shifter fiber in the tile; however the gain is less than a factor of two because of the additional attenuation in the longer fiber. More light can be collected if two independent fibers are laid in the same tile and brought independently to the PMT. There is space enough in the 30 degree crack to route the extra fibers[29] and the pixel size of the MCPMT is 4.5 mm[30], which can easily accommodate two fibers.

Recently tests have been done[27] to measure the light output from such a configuration using a realistic system of fibers, including optical connectors, and a Hamamatsu H4139 MCPMT, which is similar to the H5828 which is currently favored for the shower maximum detectors. (The main difference is the number of pixels.) A sketch of the test configuration is shown in Figure 11. The tile was 152 x 152 x 6.4 mm^3 BC404 with a 2.5 mm deep sigma pattern groove 3.2 mm from the edge and with 32 mm radius curves at the corners. This tile size is characteristic of the largest (low η) towers in the EM (see Table 1), which will tend to give less light than the smaller, higher η towers. Two pieces of mirrored 0.83 mm Y11 (250 ppm) non-S-type multiclad fibers were laid in the groove. Each green fiber was spliced to 1 m of 0.83 mm clear fiber, a length characteristic of a high η towers. A 2.5 m long 2-fiber optical "cable" of 0.9 mm clear fiber with EM- and hadron-type connectors on either end was used to simulate the optical path to the back of the plug. The cable connected to a pair of 0.3 m long 1.0 mm diameter clear fibers which routed the light either to an R4125 conventional PMT with light mixer (the tube selected for the plug upgrade calorimeter) or to the MCPMT.

Beta particles from a Ru^{106} source were used to measure the number of pe/mip. A pair of 1 mm thick trigger counters were used to gate a 15-bit LeCroy ADC with a 0.04 pC least count, and the number of photoelectrons (N_{pe}) was determined from the fraction of triggers in the pedestal. The trigger is estimated to have an accidental fraction of about 0.2%, so this method is unreliable for more than 4-5 pe's. For higher light levels the ratio of mean ADC to N_{pe}, determined from other lower light level configurations, was used to determine N_{pe}.

With the conventional PMT 10.9 pe/mip were observed, and with the MCPMT 5.6 pe/mip were observed. This ratio of two has been observed in other tests done for the shower maximum detector. Using an experimental green-extended MCPMT (H4139G-20MOD), 6.0 pe/mip were measured. Hamamatsu quotes the quantum efficiencies at 520 nm to be about 15%, 10% and 11.5% for the R4125[31], H4139[30], and H4139G-20MOD[32] respectively. The larger ratio of observed N_{pe} than the ratio of quantum efficiencies presumably reflects a poorer efficiency of the MCPMT to collect and amplify the photoelectrons, apparently only about 75% of that of the conventional PMT.

The observed 5.5-6 pe/mip is a more than the required 5 pe/mip. However, to achieve this result required the use of BC404, which is significantly more expensive than BC408, and two fibers per tile, which would complicate the assembly. BC408 is about 10% less bright than BC404[28], and using 2 turns of a single fiber yields about 20% less light than using 2

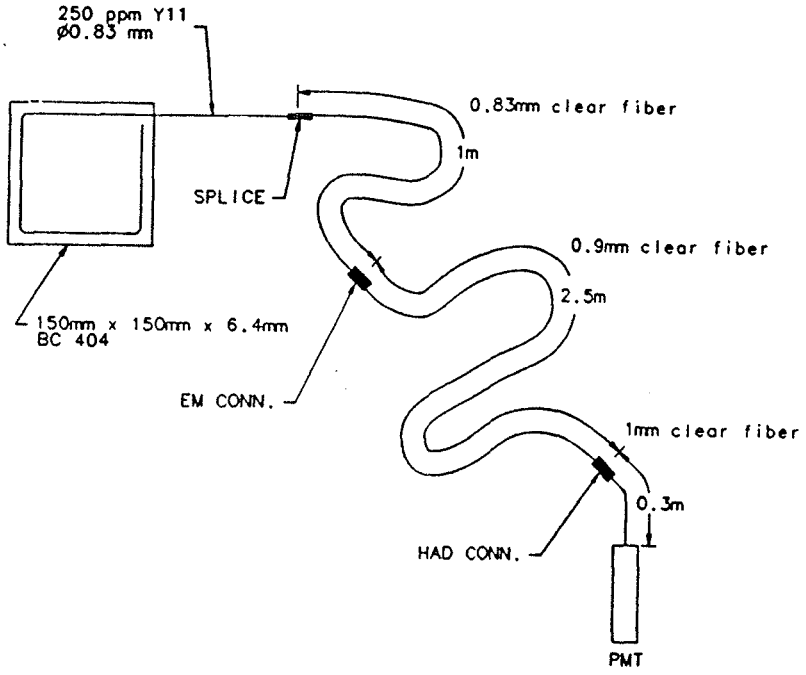

Figure 11: Tile-fiber system used for measurement of the absolute light output expected from the preshower counter.

fibers[27]. Such a configuration would result in only 4-4.5 pe/mip. Increasing the thickness of the scintillator from 6.4 mm to 10 mm increases the light output by about 35%[33], just the amount lost by going to the less expensive scintillator and 1 fiber per tile. A small sample of 10 mm BC408 has recently been obtained, and measurements with the proposed "final" configuration will be done within the next 1-2 months.

3.2.3 Preshower Scintillator Assembly ("Pizza Pan") Design

The preshower scintillator pizza pans will follow the same design as is used for the EM calorimeter pans (Figures 2 and 12). This design consists of individually cut tiles, which are sandwiched between two white plastic covers; the tiles are attached to the covers by scintillating rivets. The edges of each tile are painted white, and white PET paper is used as a reflector between the scintillator and white plastic covers. Both fibers and source tubes (used to guide a wire driven source for calibration - see below) are routed on the top surface of the top white plastic layer. Some modifications may be required if it turns out to be necessary to use two fibers per tile to get enough light. For example, it may be required to increase the thickness of the top white plastic cover by about 1 mm to allow the additional fibers to cross the source tubes. The overall preshower pan thickness will therefore be 0.8 mm (bottom cover) plus 10 mm (scintillator) plus 2.7 mm (top cover) for at total of 13.5 mm, which is 7 mm more than a standard EM pan.

The requirements on the transverse uniformity of the response of each tile have not been determined yet. By varying the depth of the fiber groove and its distance from the edge of the tile, a response uniformity of 2.5% has been achieved for the EM tile, and a similar optimization can be done for the preshower detector. The requirements on uniformity are expected to be somewhat less stringent than for the EM calorimter, since it is only a single layer. As long as the number of photoelectrons per minimum ionizing particle is large enough, the response for $\gamma - \pi^\circ$ discrimination will not be affected by non-uniformities that are somewhat larger than those in the EM calorimeter. Because the statistical fluctuations in the energy deposited by an electromagnetic particle in one layer are large (see, for example, Figures. 7 and 10), the effect of non-uniform response at the several percent level on $e^\pm - \pi^\pm$ discrimination and on calorimeter energy resolution should not be important. However, this has not been studied quantitatively yet.

3.3 Readout System

3.3.1 Multichannel Photomultiplier Tubes

Based on both cost and space considerations, it is not practical to use conventional, discrete photomultiplier tubes to read out the preshower detector. Therefore it is planned to use multichannel PMTs. If possible, we plan to use the same MCPMT as is used for the shower maximum position detector. The shower maximum group is currently evaluating MCPMTs from Hamamatsu and Philips. The Hamamatsu MCPMTs use fine mesh dynodes whose compact structure maintains the spatial information of where a photon struck the photocathode. However, the fine mesh dynodes result in a substantially worse pulse height resolution than is obtained from a conventional PMT with a linear focused dynode structure[23]. Also, because the fine mesh dynode structure allows some spreading of the

Structure of a Pizza-pan

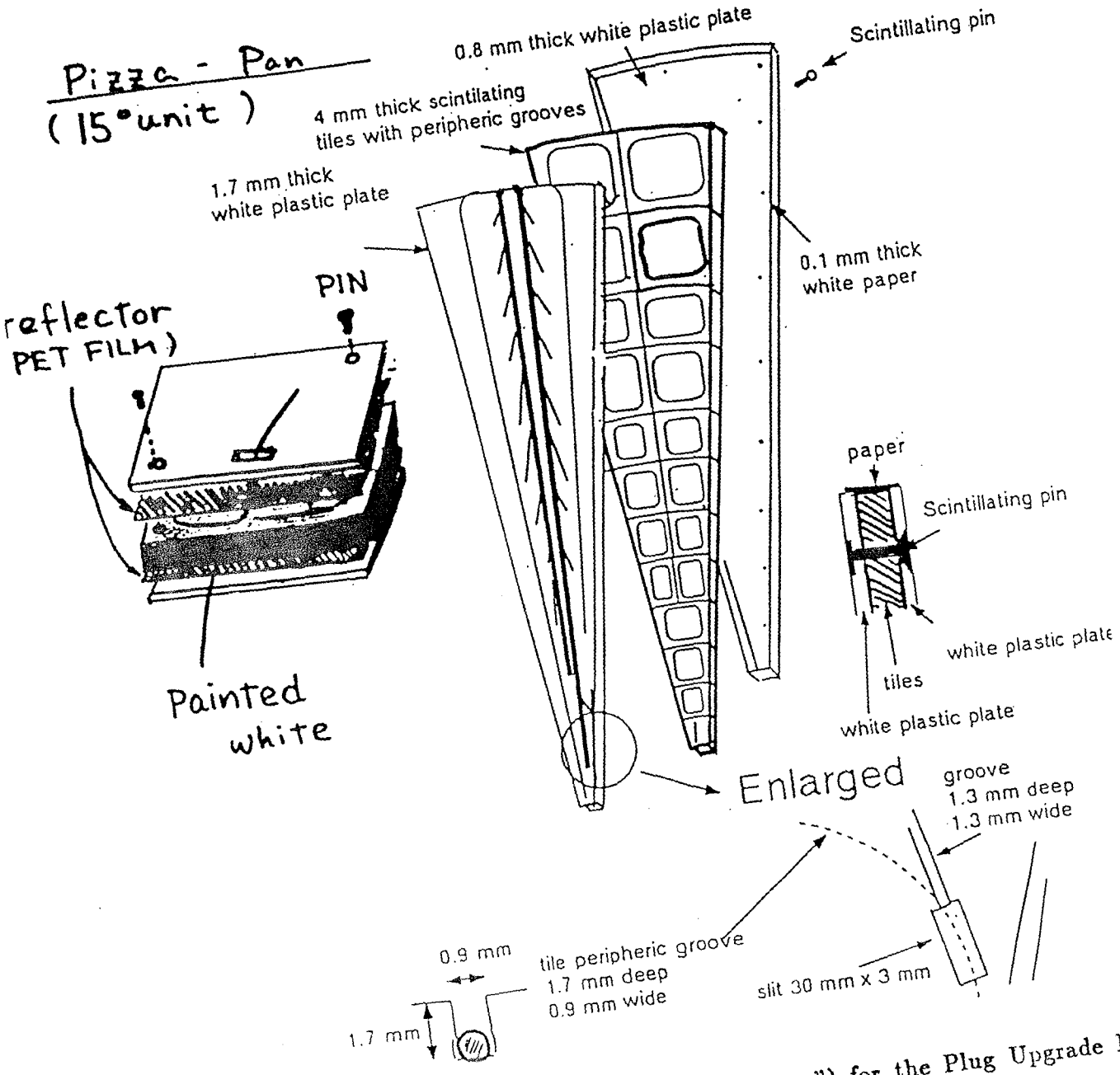

Figure 12: Design of the scintillator assembly ("pizza pan") for the Plug Upgrade EM calorimeter. A similar design is proposed for the Preshower Detector.

electrons as they are amplified, there is a few percent cross-talk between adjacent channels. The Philips tube uses a foil dynode structure that is more like the discrete dynodes of a conventional PMT. The electrons are captured and amplified in a specific channel, and the pulse height resolution is comparable to a conventional PMT. Unfortunately, the product of the quantum efficiency and the collection efficiency is only about half of that of the Hamamatsu tube. Since good efficiency for small light signals is absolutely required, the Hamamatsu tube is strongly favored despite its other shortcomings. Some details of these tubes have been discussed in Sections 3.2.1 and 3.2.2 in the context of the light yield requirements. Further details may be found in[34].

The MCPMT currently favored for the shower maximum detector is the Hamamatsu H5828[30], which has 80 channels. Another tube which uses the same dynode structure and has the same photocathode but only 64 channels is the H4139[30]. (Surprisingly, Hamamatsu quotes a higher price for the H4139 MCPMT.) Each end plug has 480 preshower tiles; therefore if the H5828 is used, 6 MCPMTs per end are required. In addition, one tube will be required for the test beam module and one spare tube will be bought, for a total of 14 MCPMTs. The shower maximum position detector will require approximately 100 MCPMTs, and we propose to buy tubes for both detectors at the same time to guarantee interchangability and to take advantage of the lower cost of buying in larger quantity.

3.3.2 Readout Electronics

Detailed studies of the electronics requirements or the ability to achieve these requirements have not been done, so the information given in this section is very preliminary. However, compared with the electronics for the calorimeter, the requirements for the preshower detector are comparatively modest. To allow good efficiency for separating photon conversions from noise, the minimum ADC sensitivity should less than 0.1 mip equivalent, say about 0.02 mip equivalent, similar to the CEM electronics. To allow the preshower energy to be summed with the calorimeter energy, the ADC must have a full scale range corresponding to the largest pulse expected from a several hundred GeV electron. Figure 13[25] is a histogram of a GEANT simulation of the number of mips in 50 GeV electron (and π^0) showers after 1.5 X_0. Figure 6 shows that the energy deposited in a preshower detector increases only modestly with increasing energy. Therefore a full scale range corresponding to 80-100 mips should be sufficient to cover the highest energy deposition expected in the PPR. The required dynamic range can be achieved with an ADC with a minimum of 12 bits. If the MCPMT run at a gain of 10^6 (compared to 10^5 which was used in the Monte Carlo studies discussed in[24]), which is well within the range of the Hamamatsu MCPMT, a 1 mip signal, which gives 5 pe's at the photocathode, gives a signal of 0.8 pC at the anode. Therefore the required least count, corresponding to 0.02 mip, is 0.016 pC, which is well within the range of current technology. It will probably be possible to meet the requirements of the PPR using the same electronics as for other calorimeter subsystems. The specifications for these systems should be developed together over the next several months.

The preshower detector could be used to enhance plug electron and photon triggers. For example, it may be possible to improve the signal to noise for a plug electron trigger by a factor of 3 or more by requiring a large pulse height in the PPR. We have not yet considered trigger issues in detail, however.

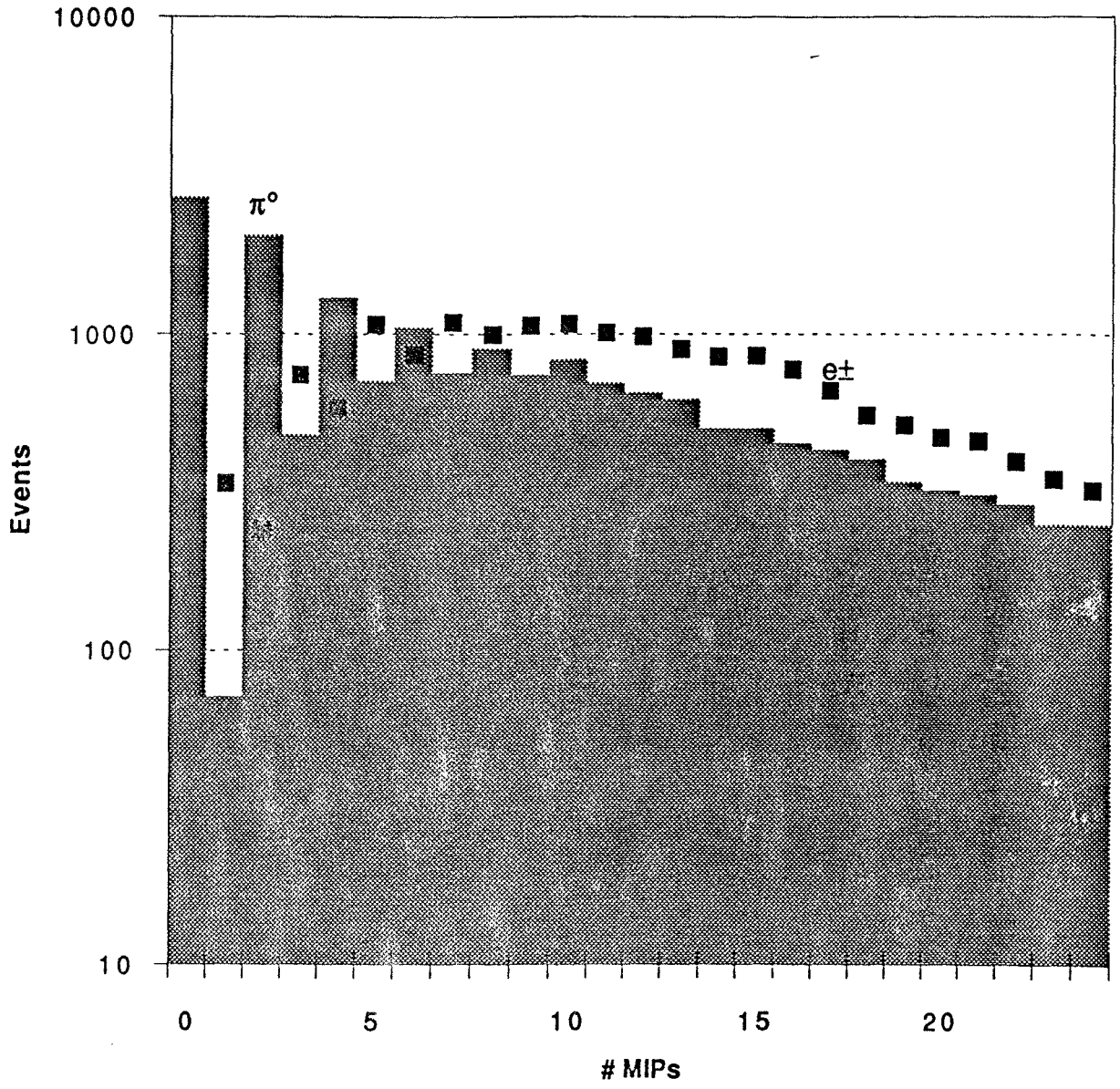

Figure 13: Distribution of the number of minimum ionizing particles for 50 GeV electron and π^0 showers after 1.5 X_0 from a GEANT simulation[25].

3.4 Modifications to the Plug Upgrade Lead Absorber

The current design of the EM calorimeter, which does not include a preshower detector, has a 6.4 mm thick stainless steel front plate followed by a full thickness absorber sheet consisting of 4.5 mm of lead clad with 0.5 mm of stainless steel on both sides before the first scintillator layer. Figure 8 shows a detail of the Plug Upgrade EM calorimeter absorbers. The gap between absorber layers is 8.8 mm. A standard EM pizza pan, which consists of 4 mm of scintillator and two white plastic covers of 1.7 mm and 0.8 mm thickness (see Figures 2 and 12), is inserted into each gap. Note that in this design, including the material before the end plug, the first sampling layer is at a depth of about 2 X_0, which should be decreased even if a preshower detector is not implemented.

We propose to reduce the thickness of the first absorber layer to put the first sampling layer at a depth of about 1.5 X_0, which can be accomplished by reducing the lead thickness to 2.0 mm. Because this first lead sheet is against the stainless steel front plate, it needs cladding on only one side. The reduced absorber layer thickness increases the gap for the preshower detector by 3.0 mm to 11.8 mm. Including a "stay clear" region, the front plate of the end plug must be at least 1752.6 mm (69.00 inches) from the interaction point. A 5 mm buffer has been defined to allow for errors, last minute design changes, etc., which moves the limit for design purposes to 1757.6 mm. In the current design the front surface of the front plate is at 1764.5 mm. Therefore there is room to increase the first EM gap by as much as an additional 6.9 mm. Summed with the increase due to the decrease in the first absorber thickness, the maximum gap possible is 8.8 + 3.0 + 6.9 mm = 18.7 mm without violating the stay clear plus buffer.

The proposed preshower pizza pan is 13.5 mm thick, which, taking into account tolerances and clearance to allow the pan to be inserted, requires an absorber gap of 15.8 mm. This is comfortably less than the maximum possible gap.

4 Expected Performance of the Plug Preshower Detector

4.1 $e - \pi^{\pm}$ Separation

The precise pion rejection factor for the plug preshower will depend on the details of the performance of the other detectors, the cuts used, and backgrounds from the underlying event, etc. The additional rejection after all other cuts can be estimated from the ratio of interaction lengths in front of the preshower and shower maximum detectors. Figure 9 shows the depth of various EM calorimeter components as a function of η for the case of a preshower at a depth at normal incidence of 1.46 X_0 and compares it with the current design which has no preshower detector and a full thickness lead sheet before the first scintillator layer. The preshower detector is at about half the depth, in terms of interaction lengths, as the shower maximum detector (0.22 λ_I and 0.40 λ_I respectively at η=2.0). Therefore the preshower detector should be able to reject approximately half the $\pi^{\pm}$s that pass EM, HAD and SMD cuts.

This simple reasoning is confirmed by SDC and CPR test beam results. In the SDC

prototype beam test[19], there was a preshower detector (PS1) after 1 X_0 (0.23 λ_I) of aluminum and a second preshower detector (PS2) after an additional 1 X_0 (0.03 λ_I) of lead. The shower maximum detector was at a depth of 8.1 X_0 (0.49 λ_I). Figure 14 shows the distributions of EM/HAD, SMD energy, and preshower energy for 15 GeV electrons and pions. Two sets of cuts ("tight" and "loose") are indicated by arrows along the horizontal axes. In this analysis no requirement was made on E/p to reflect the lack of momentum measurement in most of the plug region. Figure 15 shows the fraction of charged pions accepted versus the fraction of electrons accepted as the the preshower energy cut is varied. This is shown for both preshower layers and for both tight and loose EM/HAD and SMD cuts. The points at the upper right of each pair of curves correspond to no preshower cut. The fraction of pions rejected by the preshower detector at 2 X_0 is about 70-90% depending on the desired electron efficiency. For example, a preshower cut that has 90% efficiency for retaining electrons that passed previous cuts yields an improvement in signal to background ratio is more than a factor of 4.

In one run of the CPR beam test[20] additional copper absorber was placed in front of the test module. This put the CPR a depth along the beam direction of 1.5 X_0 (0.27 λ_I) and the CES at a depth of 6.9 X_0 (0.44 λ_I). After E_{CEM}/p and E_{CES}/p cuts, a cut on CPR pulse height that was 90% efficient for electrons rejected 62% of the pions for an improvement in signal to background of 2.4. The signal to background improvement is less than in the case SDC test beam perhaps because an additional cut on E/p was applied before analysing the pion rejection of the CPR.

4.2 Adding Preshower and Calorimeter Energy Measurements

In this section we estimate the impact of adding a preshower detector in front of the PEM. From EGS simulations and SDC test beam data, we find that the energy measured in the EM calorimeter and in the preshower detector can be summed off line to give an energy resolution as good as or better than would be obtained if a standard calorimeter scintillator layer were present in the first (preshower) absorber gap. There is a small loss in resolution at the trigger level, but not by enough to cause a significant loss in the trigger efficiency or increase in rate.

The preshower tile makes the first sample 1.5 radiation lengths into the shower. The first PEM tile is one sampling layer deeper at 2.4 radiation lengths. The disadvantage of this configuration is that the PEM energy resolution, at the trigger level, will be degraded by the 2.4 X_0 of material before the first PEM sampling layer. To estimate the effect of starting the PEM after several radiation lengths of dead material, we use test beam data from a SDC test beam module of a similar tile/fiber calorimeter design[19]. The SDC calorimeter consisted of 20 samplings every 1 X_0 of lead with 4 mm thick scintillator tiles read out by 1 mm diameter WLS fibers spliced to clear fibers, with each 10×10 cm tower bundled to one phototube. The resolution was expected to be $\sim 20\%/\sqrt{E}$, although the momentum spread of the beam degraded the measured resolution. Figure 16 shows the measured EM energy resolution versus radiation lengths in front of the first electromagnetic calorimeter (EMC) scintillator sampling for 15, 27, and 35 GeV electron showers. The resolution degradation is greatest at low energies: for 15 GeV electrons the resolution (σ_E/E) varies from 5.1% for 1 X_0 to 6.8% with 2 X_0 and 7.6% with 3 X_0 of material in front.

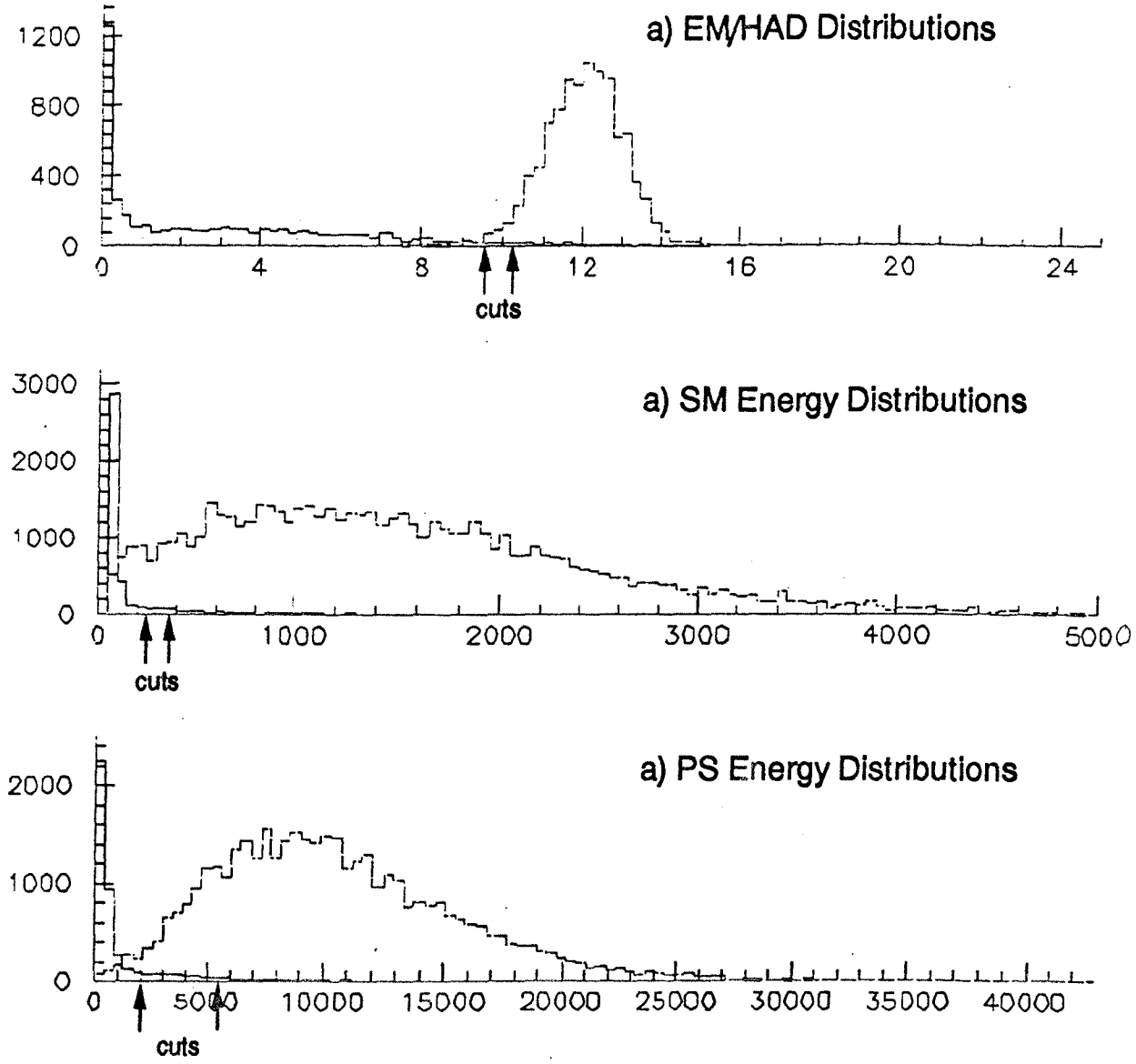

Figure 14: Distributions of EM/HAD, shower maximum detector energy, and preshower energy for 15 GeV electrons and pions in an SDC beam test. "Tight" and "loose" cuts are indicated by arrows along the horizontal axes.

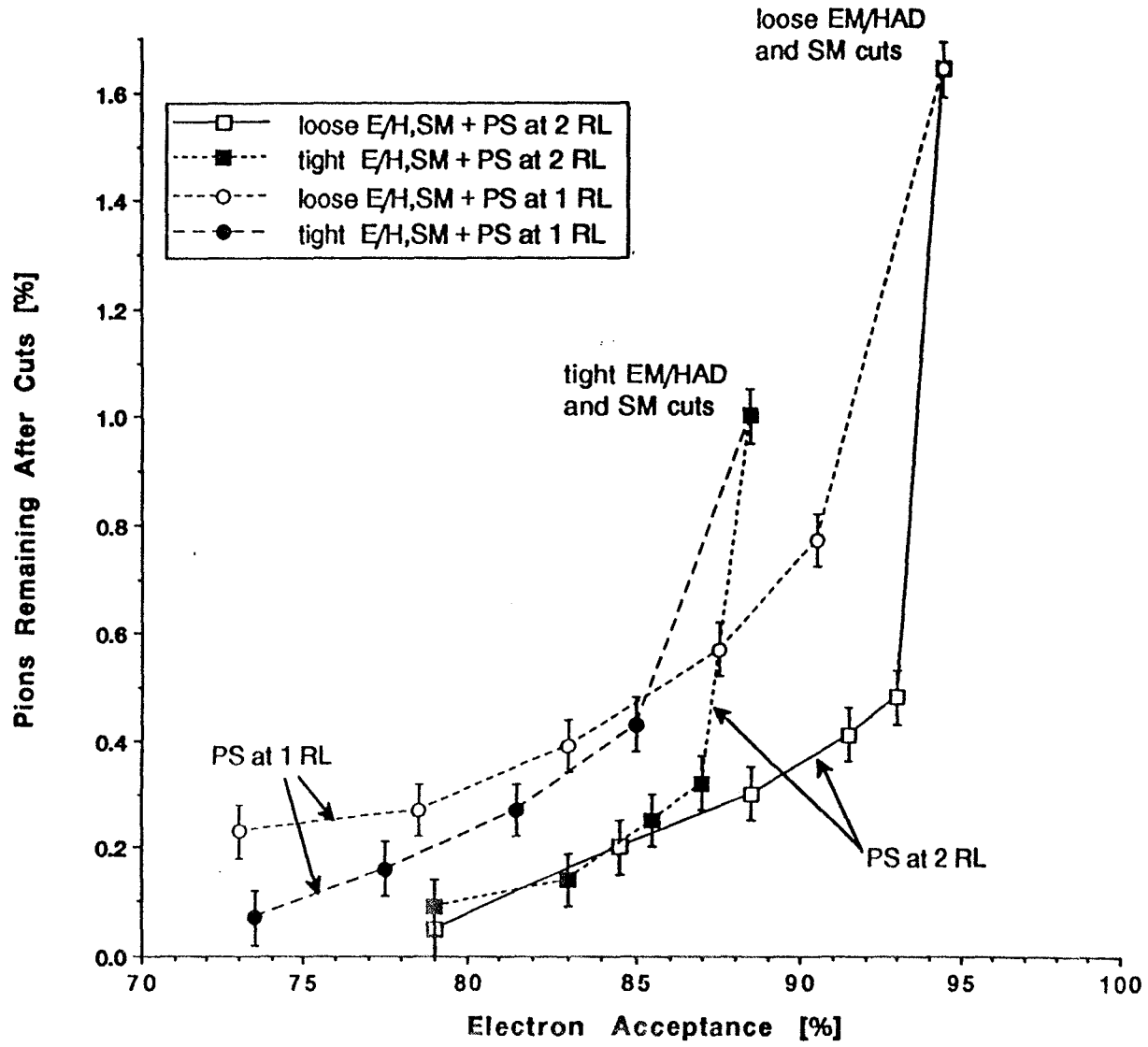

Figure 15: Pion efficiency versus electron efficiency as the preshower energy cut is varied in an SDC beam test. Cuts on HAD/EM and shower maximum detector energy have been applied before the preshower cuts. The point at the right corresponds to no preshower cut.

An EGS simulation of the EM energy resolution correction using a preshower detector after 1 X_0 of Aluminum has been performed[35]. The simulated EMC had 1/8" lead ($\sim$ $0.5X_0$) samples using 2.5 mm thick scintillator, up to a depth of 25 X_0 with energy resolution of approximately $12\%/\sqrt{E}$. To compare this simulation in a more accurate way with the Plug Upgrade PEM, we reanalyzed the simulated showers assuming sampling every 1/4" of lead by using only every other scintillator layer. This gives an energy resolution of approximately $19\%/\sqrt{E}$. Using these simulated showers, Figure 17 shows the fraction of EMC energy, compared to the EMC energy summed over all layers (with the 1 X_0 Aluminum in front), versus radiation lengths of material in front of the first active scintillator layer. The EMC contains 97% and 98% of the energy, for 12.5 and 25 GeV electrons respectively, after 2.5 X_0. Figure 18 shows the corresponding energy resolution for the EGS EMC versus radiation lengths in front of the first active layer. Comparing an EMC that starts sampling at 1.5 X_0 with one that starts at 2.5 X_0, the resolution degrades from 5.1% to 5.5% for 12.5 GeV and from 3.7% to 3.9% for 25 GeV electrons.

This deterioration in EMC energy resolution due to the lack of sampling within the first 2.4 X_0 will effect the trigger. However, offline it can be corrected, to better than the resolution after 1.5 X_0, by adding the properly weighted preshower energy to the EMC energy. In the EGS simulation, the first active layer, after 1 X_0 (10.7 cm) aluminum, was defined to be the preshower detector. The authors of[35] define the preshower weight as multiples of the energy deposited in the preshower layer, so that a weight of 1.0 corresponds to just adding the layer equally to all other sampling layers. The authors find that the EMC resolution can be improved by adding in the preshower with optimal weights ranging from 1.3 (100 GeV) to 2.0 (12.5 GeV) for particles at normal incidence, and 1.5 (100 GeV) to 3.0 (12.5 GeV) for particles incident at 30° with respect to normal. The optimal preshower weight seems to decrease with increasing electron energy.

Data were also taken with the SDC prototype EMC with a preshower detector in front[19]. The preshower data had 1 X_0 of Aluminum, a 1 X_0 thick lead sheet and 6 ribbons of 1 mm diameter scintillating fibers read out together as the preshower signal, all in front of the EMC described above. Because the preshower detector can not easily be normalized to a single EMC tile, the preshower was cross-calibrated with the EMC energy. Figure 19 shows the preshower energy versus the EMC energy where the points are the mean preshower energy deposited for each EMC energy bin, and the error bars represent the error on the mean. The preshower energy is cross-calibrated using the slope of the anticorrelation shown in this figure.

The proper preshower weight can then be accurately determined offline by using variable preshower weights when adding to the EMC energy and finding the minimum of the corrected energy resolution. Figure 20 shows an example of preshower-corrected EMC energy resolution versus preshower weight from SDC test beam data[19]. For this particular configuration, the optimal preshower weight was approximately 0.2. A preshower weight of 2.0, for the EGS simulation data described above, corresponds to a weight of approximately 0.2 when the preshower is cross-calibrated with the EMC. The optimal preshower weight depends on the amount of material in front of the preshower, the relative light yield of the preshower tile compared to a EMC tile, and the EMC sampling ratio (X_0 per layer). Figure 21 shows data on the EMC energy resolution improvement provided by combining the preshower energy. For example, the energy resolution for 15 (50) GeV electrons with 2 X_0

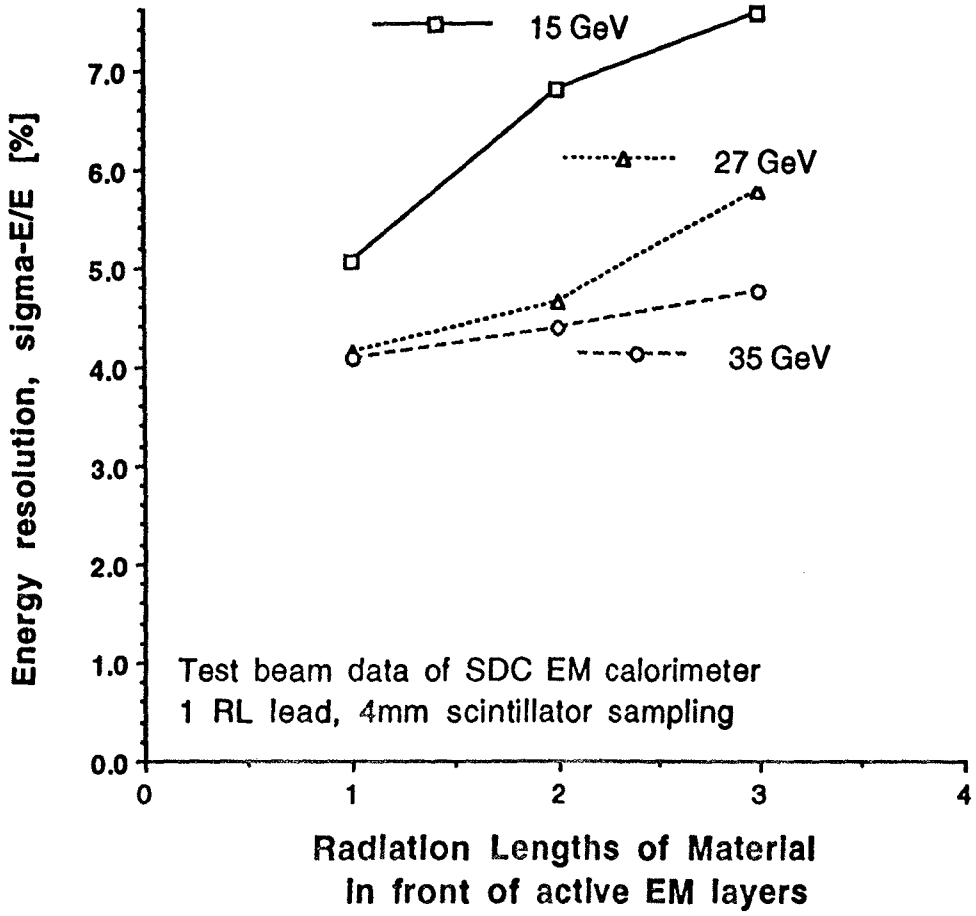

Figure 16: Energy resolution measured in an SDC beam test as a function of the number of radiation lengths of material in front of the first sampling layer.

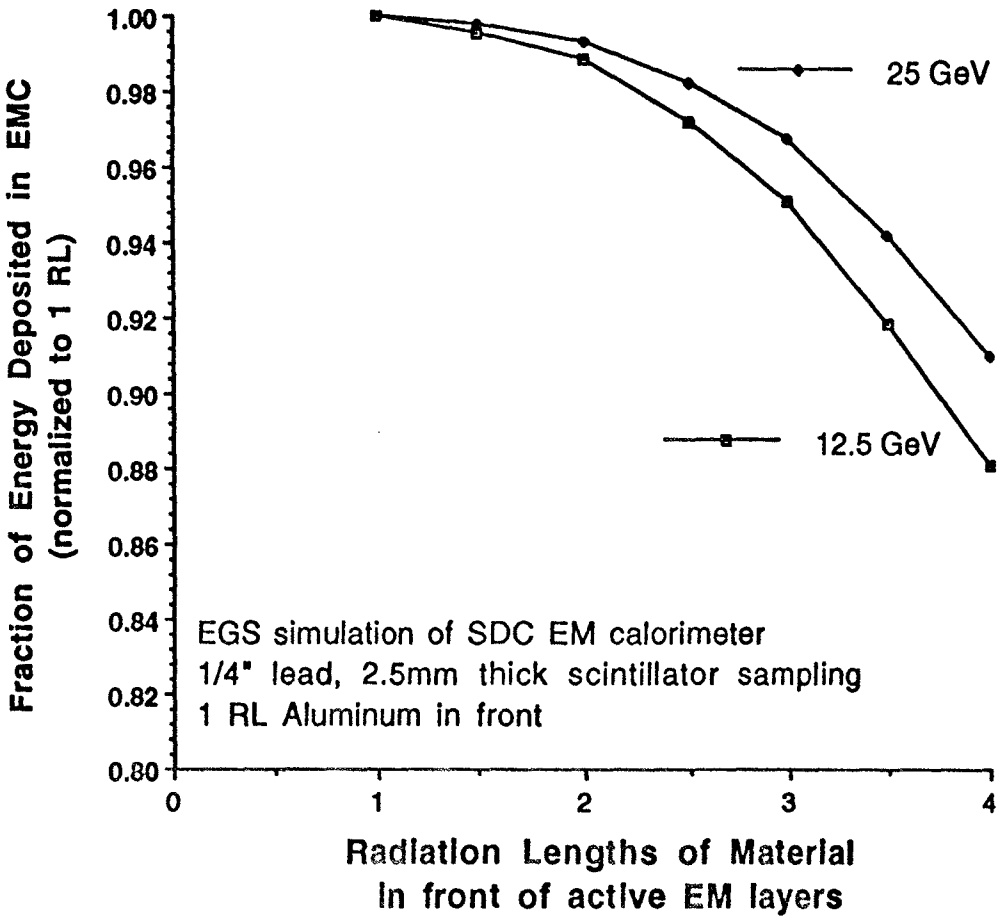

Figure 17: The fraction of electromagnetic energy observed in an EGS simulation of a EM calorimeter as a function of the amount of material in front of the first sampling layer. The observed energy fraction is normalized to the first point at a depth of 1 X_0.

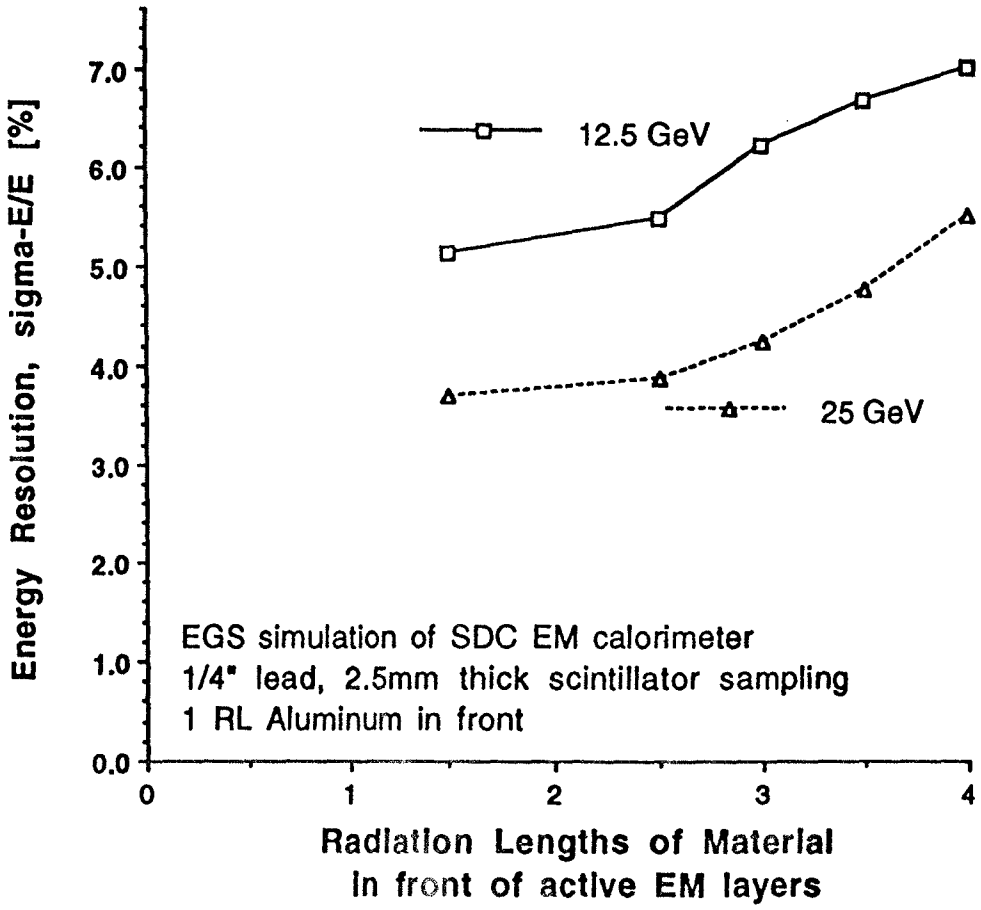

Figure 18: Energy resolution measured in an EGS simulation as a function of the number of radiation lengths of material in front of the first sampling layer.

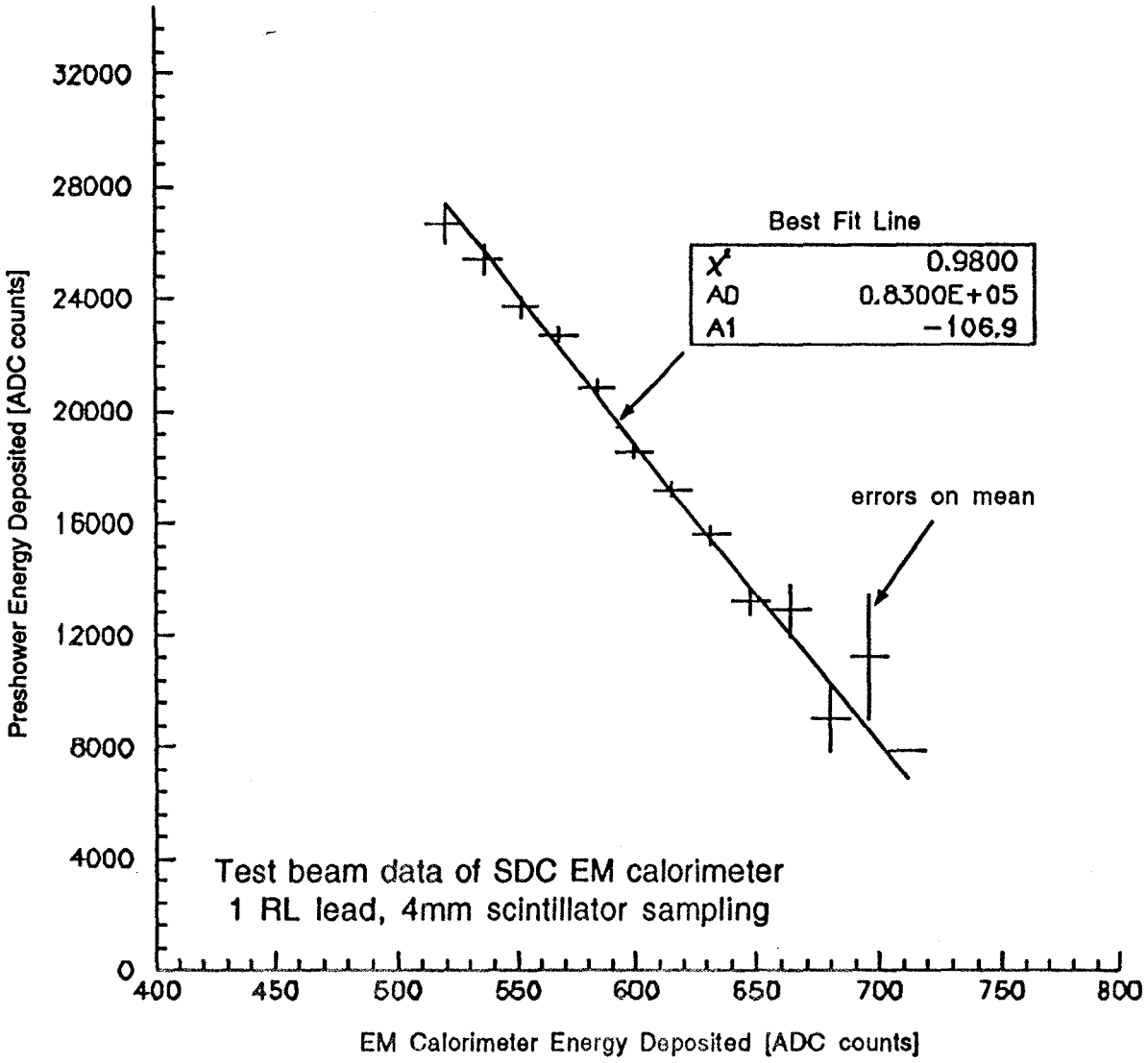

Figure 19: Mean energy deposited in the preshower detector versus the mean energy deposited in the EM calorimeter for a sample of 27 GeV electrons in an SDC beam test.

in front is 7.6% (4.4%) uncorrected, and 6.6% (3.6%) with the preshower correction.

Therefore, offline the energy measured in the EM calorimeter and the preshower detector can be combined to give an energy resolution that is at least as good as would be obtained if a standard calorimeter scintillator layer were present in the first (preshower) absorber gap. At the trigger level, however, there will be some loss of information, since it is not practical to combine the EM and preshower energies in hardware. The few percent of energy that is not measured (see Figure 17) will cause an insignificant shift in the effective trigger threshold. The poorer resolution will cause the trigger threshold to be softer. If the threshold is set to be fully efficient at a particular energy, the poorer resolution in the case that the first sample is at 2.4 X_0 will allow more events of lower energy to satisfy the trigger and therefore drive up the trigger rate. However, the expected degradation of resolution is not large. For example, the SDC test beam data in Figure 16, which are more pessimistic than the simulation shown in Figure 18, show the resolution to degrade from 6% to 7.2% at 15 GeV (E_T = 4 GeV/c at $\eta = 2$), or from 0.9 GeV to 1.08 GeV. Thus an increase of the trigger threshold by a few hundred MeV should be sufficient to set the trigger rate at the level it would have been with better energy resolution.

The resolution at the trigger level could be made almost as good as that off-line by placing a standard EM scintillator layer, which would be read out along with the rest of the calorimeter, in the first gap along with the preshower detector. This, however, adds additional complication and expense to the assembly, and would require the first absorber gap to be at least 20 mm, which is larger than the 18.9 mm that is available (see Section 3.4). Since there is little information loss at the trigger level and essentially none after offline analysis if there is only preshower readout from the first gap, there is no reason to pursue this option.

4.3 Background Occupancy in Direct Photon Events

Calculations to determine the required number of photoelectrons per minimum ionizing particle have shown[24] that a noise occupancy (that is, the probability of seeing a signal when there is no photon conversion) in a preshower cell of 1% results in a systematic error of 0.7% in determining the photon fraction in a sample of neutral showers, and that the systematic error is linear in the occupancy. Occupancy can arise from beam related backgrounds as well as phototube noise. The background occupancy from the underlying event plus additional minimum bias interactions in the same bunch crossing can be estimated from the measured charged particle multiplicity per unit of pseudorapidity. CDF has measured $dN_{ch}/d\eta$ at $\sqrt{s}$ = 1.8 TeV to vary from 4.2 to 4.8, with an average of 4.5, in the plug region[36]. Extrapolating to $\sqrt{s}$ = 2.0 TeV gives $< dN_{ch}/d\eta > = 4.6$. The usual assumption is that $dN_{neutral}/d\eta$ = 0.5 x $dN_{ch}/d\eta$, or 2.3 π^0 per unit of pseudorapidity. Assuming all π^0s to convert in the preradiator (with 1.5 X_0 the actual number is about 90%), then the π^0 occupancy per interaction in one preshower cell varies from 0.5% to 0.9% within the $\Delta\phi = 7.5°$ tiles ($1.1 < \eta < 2.1$) and from 2.1% to 5.0% in the 15° tiles ($2.1 < \eta < 3.5$). This calculation is plotted in Figure 22. Under some foreseen combinations of luminosity and number of bunches, the mean number of interactions per crossing could be as high as 3. This would give an occupancy per crossing (and hence per event) 3 times these values.

However, the presence of most extra π^0s within a preshower tile can be identified by

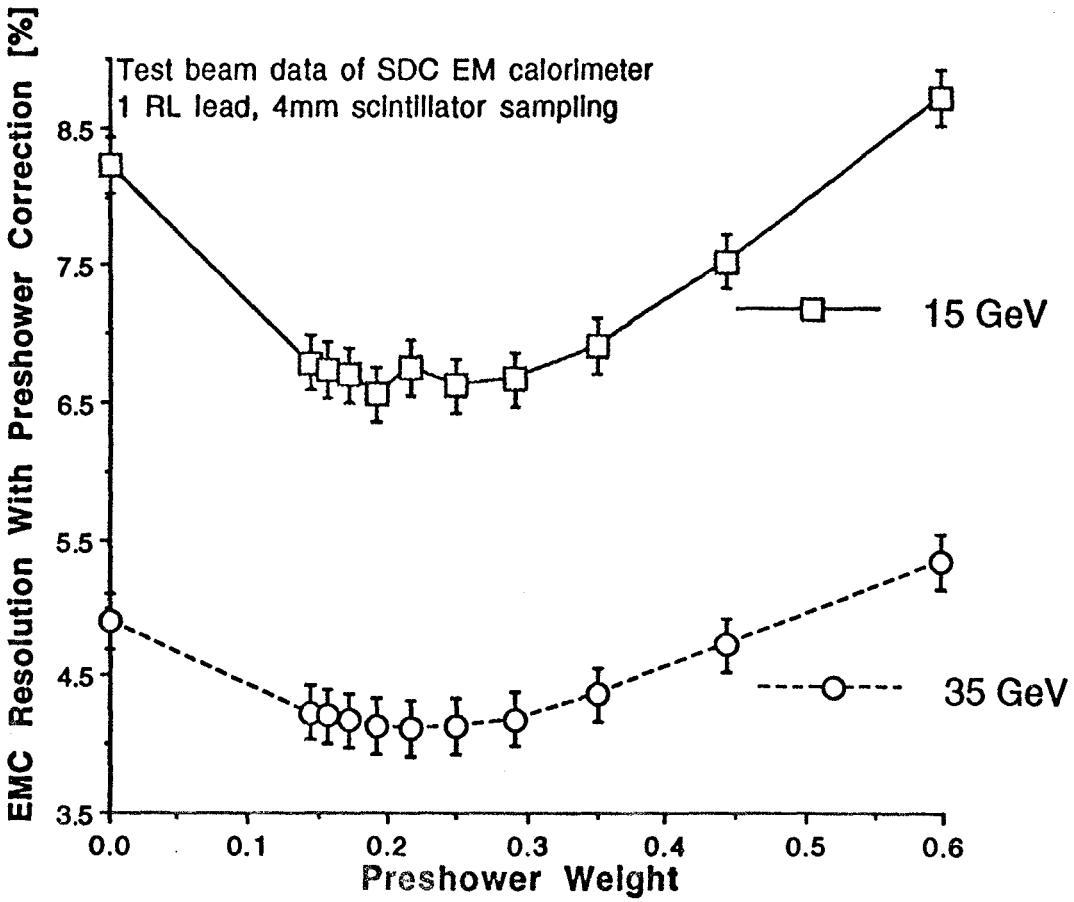

Figure 20: Measured energy resolution as a function of the weight applied to the preshower energy in summing it with the electromagnetic calorimeter energy in an SDC beam test. (See text for the definition of the weighting factor.)

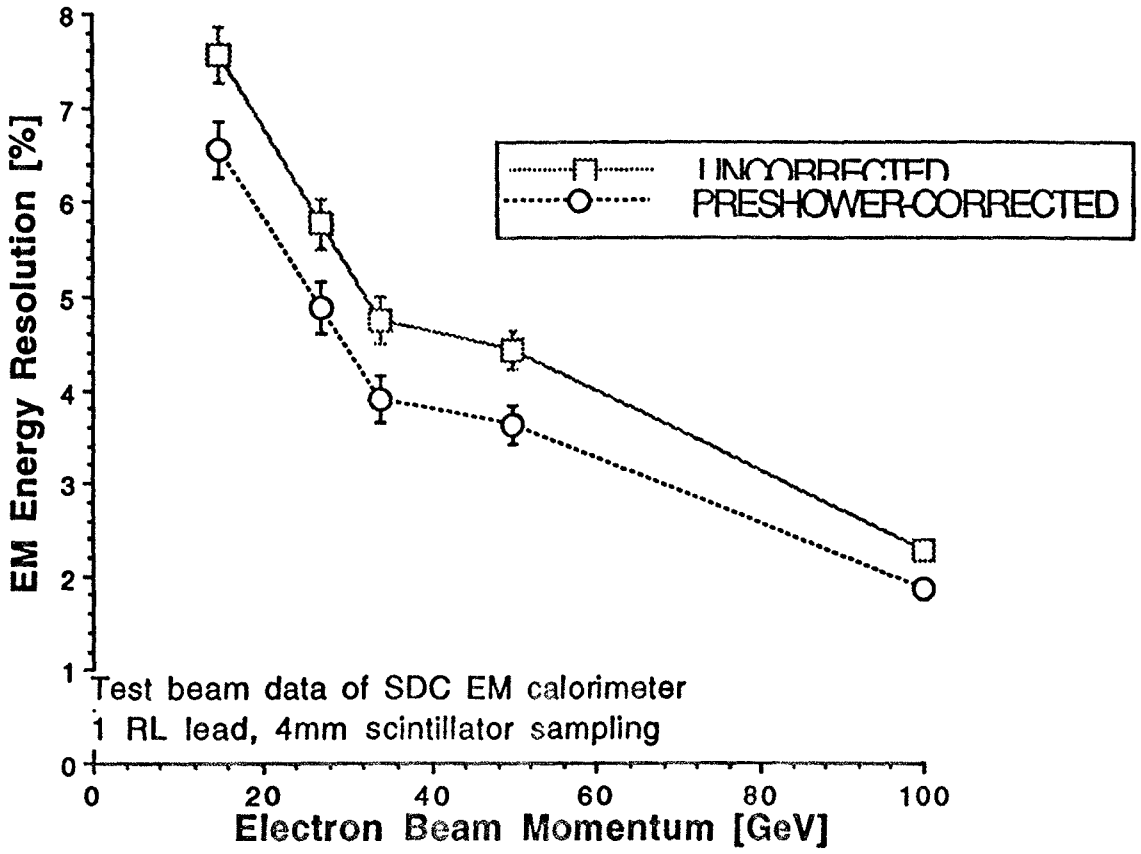

Figure 21: Measured energy resolution in a beam test of an SDC electromagnetic calorimeter prototype with and without the addition of the energy in a preshower detector at a depth of 2 X_0 (first EM sampling layer at 3 X_0.)

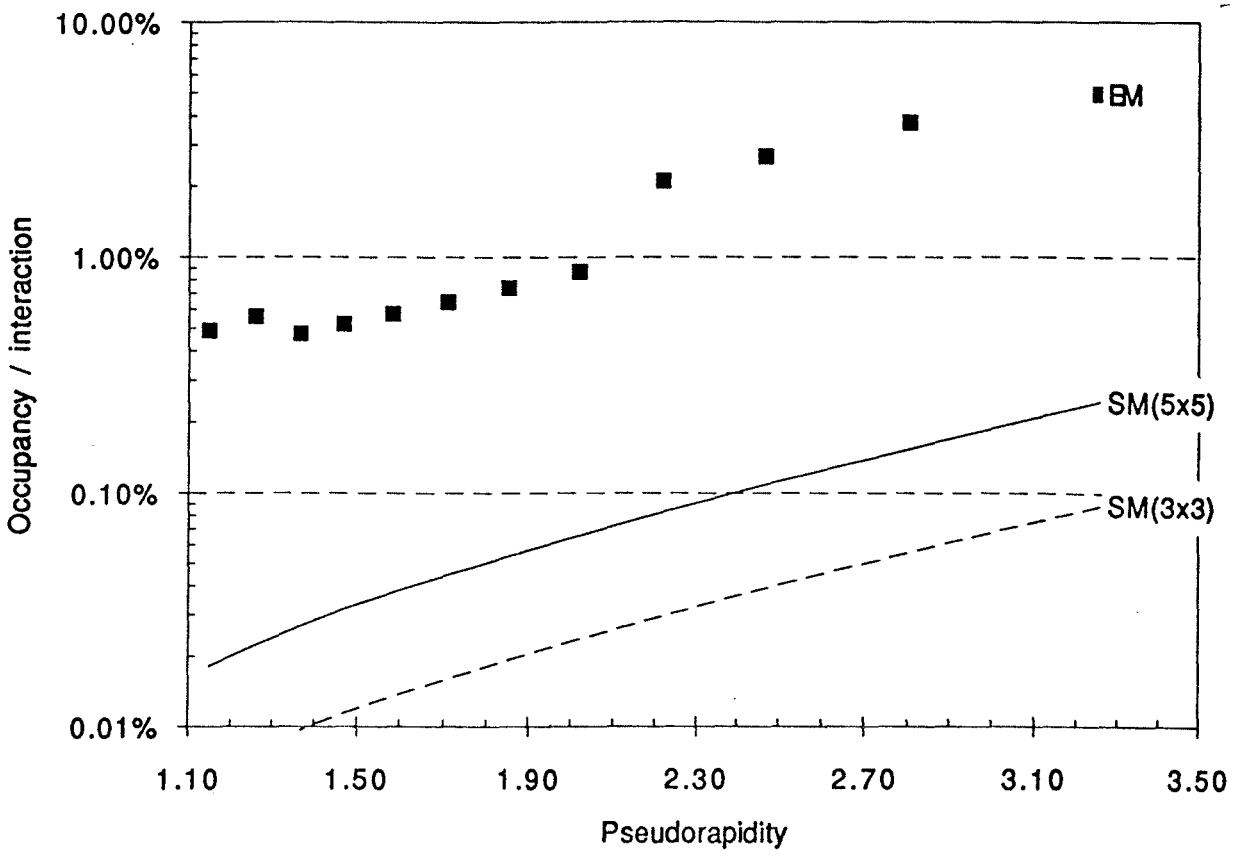

Figure 22: Occupancy in the preshower detector per interaction from minimum bias events, assuming $dN_{\pi^0}/d\eta = 2.3$. The closed squares represent the occupancy in a preshower tile assuming that both decay photons from the π^0 enter the same tile and that at least one converts. The solid and dashed lines are the occupancy due to photons from π^0 decay within 5 x 5 and 3 x 3 strip crossing area.

the signature of extra photons in the shower max detector. Events with multiple photons in one preshower cell can therefore be rejected from a single photon analysis, resulting in a loss of efficiency but no systematic error on the photon fraction measurement. There is still the background occupancy which consists of additional photons which overlap the photon of interest such that their presence cannot be identified by the shower maximum detector. Figure 22 shows the photon occupancy from minimum bias π^0s assuming the shower maximum detector "area of confusion" is the diamond shaped intersection of 3 or 5 strip roads in the two SMD views. (The FWHM of a photon shower is on the order of 1 strip.) The occupancy/interaction within the 5 x 5 strip "area of confusion" varies from 0.02% at $\eta = 1.1$ to 0.3% at $\eta = 3.5$. This will result in a negligible systematic error in determining the photon fraction in a sample of neutral showers.

There will presumably also be beam related low energy "junk" which does not give a SMD signature but does deposit energy in the preshower. Such "junk" is observable in the CPR with an occupancy of 12% per half wedge[25]. If this rate is η independent, then the "junk" occupancy in the PPR would vary from 1.1% to 2.2% in the 7.5° towers and from 5% to 12% in the 15° towers. This background is measured and subtracted in the analysis of CPR data and does not result in a major systematic error. Depending on the energy spectrum of this low energy "junk," the PPR may be substantially less sensitive to it than the CPR, since the the threshold, in terms of energy deposited in the detecting device, is almost 1000 times higher in scintillator than in a gas detector. (At normal incidence a minimum ionizing particle deposits about 2 keV crossing the CPR wire chamber and about 2 MeV crossing 10 mm of scintillator.)

5 Calibration

The preshower detector requires several types of calibrations: calibration of the response to minimum ionizing particles, which is used to set the thresholds for detecting photon conversions and for separating electrons from non-showering particles (pions), measurement of the noise spectrum and occupancy, including both PMT noise and signal from the underlying event, calibration of the energy response for combining the preshower and calorimeter energies, calibration of the stability of the MCPMT gain, and measurement of the total preradiator thickness including the material upstream of the plug.

The response of the preshower detector to minimum ionizing particles can be measured before the plug upgrade EM calorimeter is installed in CDF using cosmic rays in a planned calibration period with the plug upgrade EM calorimeter oriented in the horizontal plane at B0. The response of the test beam module preshower layer can be calibrated using the muon content of the test beam as well as test beam pions which give a minimum ionizing signature in the EM calorimeter. The test beam module response can be cross-calibrated with the main calorimeter by taking cosmic ray runs with the test beam module. With the EM calorimeter installed in CDF, the device can be calibrated using cosmic rays also, although the rate will be low. In addition, isolated charged particles giving a minimum ionizing signal in the EM calorimeter, principally non-interacting pions, can be used. Once the response to minimum ionizing particles has been well established, changes can be tracked using the movable wire source and laser stability monitoring systems (see below).

The PMT noise spectrum will be measured as often as necessary in special pedestal runs. The additional occupancy due to π^0s from the underlying event and any other beam related backgrounds can only be measured from the data themselves and will be a function of the instantaneous luminosity, the number of bunches, and perhaps other accelerator parameters or conditions.

The energy response of the preshower detector is ultimately calibrated from test beam data using the test beam module. As with the rest of the plug upgrade calorimeter, it is not planned to do a test beam calibration of the actual device to be used in CDF. Rather a "carbon-copy" test beam module will be used which will consist of 60° of the hadron calorimeter and 45° of the EM calorimeter, including the preshower detector. Based on the test beam data the proper weighting of the energy in the preshower with respect to the calorimeter will be determined. The test beam calibration will be transferred to the real plug by measuring the response of each device to cosmic rays and to a Cs^{137} source, which can be moved past each tile, including the preshower tiles, using a wire source driver[37]. Therefore it is necessary to install source tubes into the preshower scintillator pizza pan. All of the PEM layers can be accessed by the source when the plug is removed from CDF, but only a few will be accessible when the plug is installed. It is planned that the preshower detector will be one of the layers that is accesible at all times.

Variations in the response of the MCPMT can be calibrated using the laser calibration system that is currently under design for the rest of the PMT system[37]. Light from the laser will be routed to one or a few pixels of the MCPMT and will be used to monitor shifts in the average response. Shifts of individual pixels, of course, cannot be tracked this way. Measurements still need to be done to determine how well the response of different pixels track each other with time, and from this to determine how many pixels need to be illuminated by the laser. Since the MCPMT pixels are large enough to accomodate up to 4 fibers, calibration fibers can share pixels with fibers from the preshower detector and as many pixels as necessary can be illuminated by the laser.

The preradiator thickness, including upstream material, can be measured using the existing gas PEM calorimeter for the configuration during Run Ib, which is more like the Run II conditions than those during the 1988-89, by repeating the analysis in[21]. A similar analysis can be done with the upgrade plug calorimeter by looking at the energy deposited by electrons from W and Z decays in the preshower, the shower maximum detector, and the EM calorimeter. This method can be calibrated in the test beam by comparing the response with and without extra material placed upstream of the test beam module. This type of test beam calibration run is important for both $\gamma - \pi^0$ and e -$\pi^{\pm}$ separation. Ultimately the effective thickness of the preradiator for use in determining the γ fraction in a sample of neutral showers will be determined using π^0s and ηs identified with the shower maximum detector as is done for the Central Preradiator[4, 22].

6 Cost Estimate and Schedule

The cost of including a Preshower Detector as part of the Plug Upgrade is relatively modest. The total estimated cost is \$445K, which is only a few percent of the total Plug Upgrade cost and is less than 1/3 of the remaining contingency. Table 3 summarizes the

estimated cost of the Plug Preshower. This is the cost rollup from a more detailed WBS for this project.

The cost estimates for many of the major elements are based on actual costs for similar items in the PEM calorimeter or on recent vendor quotes. Therefore a relatively modest contingency has been applied to most items. The cost of the scintillator assemblies is assumed to be the same as the actual cost of the EM pizza pans, which are being manufactured by a Japanese company, except for the greater cost of the scintillator itself. The scintillator cost is based on a quote from Bicron for 10 mm BC408 in a quantity appropriate for the preshower detector. The cost of the optical cables is assumed to be the same as that for the rest of the plug and is based (conservatively) on the assumption of 2 WLS fibers per tile. The preradiator cost includes the cost of special spacers that would have to be made for the larger gap than is in the original design plus the cost of the lead itself. The MCPMT system cost includes multichannel PMTs, high voltage supplies, and cables. The cost of the MCPMTs dominates this item, and is based on a price quote from Hamamatsu assuming that we buy the MCPMTs for the preshower along with those for the shower maximum position detector. (If the purchases are made separately the lower quantity would lead to a higher price per tube.) It is worth noting here that MCPMTs are relatively newly on the market, and there is reason to hope that by the time we are required to purchase them their cost may have dropped. The item with the largest uncertainty is the readout electronics, since the electronics have not been designed. A conservative cost estimate of \$150/channel plus a 30% contingency has been applied. The cost of the test beam module is a scaled sum of the costs of each of the other items.

Table 3: Plug Upgrade Preshower Detector Cost Estimate (K\$)

Element	M&S	Labor	Contingency	Total	FY94	FY95	FY96
Scintillator assemblies	55.7	8.1	10%	70.1	70.1		
Optical Cables	12.3	0	10%	13.6		13.6	
MCPMT System	127.8	11.6	20%	167.3			167.3
Preradiator Lead	15.8	0.6	10%	18.0	18.0		
Installation	0.5	4.6	20%	6.2		6.2	
Electronics	115.2	0.0	30%	149.8			149.8
Test Beam Module	13.0	3.9	20%	20.3	20.3		
Total	340.2	28.9	21%	445.2	108.4	19.7	317.0

The scope of this project is relatively modest, and its schedule will be determined by funding and by the requirement that it remain coordinated with the rest of the Plug Upgrade project. No technical difficulties are anticipated which would affect the schedule. Table 4 summarizes the major milestones of the Plug Upgrade project which are relevant to the preshower detector construction. This schedule is based on the Fermilab Long Range Schedule dated September 13, 1993, which shows a fixed target run from July, 1995 to May, 1996, and Collider Run IIa beginning in October 1996. A rough breakdown of which costs

need to be accrued in which year is given in Table 3. (This is a first pass estimate which assigns all of the cost of each major item to one year. It is possible to make a more detailed breakdown within each major item, but this is not anticipated to change the funding profile drastically.)

If the preshower detector is to be implemented, the lead stack must be built with this in mind. The lead stack for the test beam module will be built first, followed by the two PEM modules. If the schedule shown in Table 4 is to be followed, the components for the preradiator must be bought soon. It is not required to have any of the scintillator assemblies delivered until the first half of calendar 1995 (to allow inclusion in the test beam module). However, we propose to buy the scintillator and have the pizza pans made this year to take advantage of using the same company that made the PEM pizza pans while they are still set up to do this work. The optical cables, whose manufacture for the rest of the plug upgrade will extend well into FY95, can be purchased next year. A sufficient number of multichannel PMTs are currently owned by Plug Upgrade collaborating institutions that it may be unnecessary to purchase any additional ones for the test beam run. Electronics other than the final design will probably be used for the test beam run. The bulk of the MCPMT and readout electronics purchases can be made as late as the beginning of FY96. However, to insure that a reasonable amount of cosmic ray testing data are collected, we must buy them as early as possible in FY96.

Table 4: Plug Upgrade Project Milestones Relevant to the PPR Schedule

Milestone	Date
Begin lead stack assembly for the test beam module	March, 1994
Begin scintillator insertion in the test beam module	July, 1994
Begin lead stack assembly for first PEM	May, 1994
Begin scintillator insertion in the PEM	August, 1994
Begin cosmic ray test run with the first PEM	November, 1994
Begin test beam run	July, 1995
Begin to mount first PEM on the plug	May, 1996

References

[1] F. Abe et al.,"Measurement of the Isolated Prompt Photon Cross Section in $\bar{p}p$ Collisions at $\sqrt{s} = 1.8$ TeV," *Phys. Rev. Lett.* 68(1992)2734; F. Abe et al., "A Prompt Photon Cross Section Measurement in $\bar{p}p$ Collisions at $\sqrt{s} = 1.8$ TeV," Fermilab-Pub-92/001-E, submitted to *Physical Review D.*

[2] P. Aurenche, R. Baier, and M. Fontannaz, "Prompt Photon Production at Colliders," *Phys. Rev. D*42(1990)1440.

[3] J. Huston, talk at Workshop on Small x Physics, Fermilab, 1992.

[4] F. Abe et al., "Direct Photon Results from CDF," International Symposium on Lepton and Photon Interactions, Cornell, Ithaca, NY, August 10-15, 1993. Fermilab-Conf-93/202-E.

[5] F. Abe et al., "Prompt Photon Center of Mass Angular Distributions in $\bar{p}p$ Collisions at $\sqrt{s} = 1.8$ TeV," *Phys. Rev. Lett.* **71**(1993)679.

[6] R. Oishi, B. Flaugher, and S. Kuhlmann, "Analysis of Charm + Photon Events (I)," CDF Note 2234, September 18, 1993.

[7] R. Hamilton, D. Crane, B. Flaugher, J. Huth, S. Kuhlmann, and J. Troconiz, "A Measurement of the Photon-Muon Cross Section," CDF Note 2239, September 21, 1993.

[8] F. Abe et al., "Measurement of the Cross Section for Production of Two Isolated Prompt Photons in $\bar{p}p$ Collisions at $\sqrt{s} = 1.8$ TeV," *Phys. Rev. Lett.* **70**(1993)2232.

[9] P. Maas, "A Study of Events Containing a Photon and Two Jets," CDF Note 2074, May 1993.

[10] R. Blair, "The Diphoton Rate in the '92-'93 Sample (A First Look)," CDF Note 2070, May 1993.

[11] "Search for Excited Quarks in $\bar{p}p$ Collisions at $\sqrt{s} = 1.8$ TeV," International Symposium on Lepton and Photon Interactions, Cornell, Ithaca, NY, August 10-15, 1993. Fermilab-Conf-93/205-E.

[12] D. Benjamin, et al., "Measurement of σ * BR(W + γ) and σ * BR(Z +γ) in the Electron and Muon Channels in $\sqrt{s} = 1.8$ TeV $\bar{p}p$ Collisions," CDF Note 1941, May 1993.

[13] Barry Wicklund, transparencies from talk on b-quark cross section at CDF Collaboration Meeting, Oct. 8, 1993. Copies available from Carol Picciolo.

[14] C. Campagnari et al., "Search for Top in the Lepton + Jets Channel With a Lepton Tag," CDF Notes 1961, 2161, and 2174.

[15] F. Abe, et al., "Measurement of the Bottom-Quark Production Cross Section Using Semileptonic Decay Electrons in $p\bar{p}$ Collisions at $\sqrt{s} = 1.8$ TeV," *Phys. Rev. Lett.* **71**(1993)500.

[16] F. Abe, et al., "Measurement of $B^0\bar{B}^0$ Mixing at the Fermilab Tevatron Collider," *Phys. Rev. Lett.* **67**(1991)3351.

[17] Bob Mattingly, "The B-Bar Content of High Mass $e\mu$ events," CDF 2190, 1993.

[18] Fritz Dejong, transparencies of talk on B physics at Aspen PAC meeting, June 1993. Copies available from Carol Picciolo.

[19] M. Hulbert, et al., "Effect of a Preshower Detector on Calorimetry Performance," SDC-92-294, accepted for publication in NIM (1993).

[20] S. Kuhlmann, "Central Preradiator Detector Tests," CDF Note 1248, July 1990.

[21] M. Takano, "Longitudinal Shower Profile of Electrons in Plug EM Calorimeter," CDF Note 1165, April 13, 1990.

[22] R. Harris, "Measurement of η/π^0 from Isolated Decays into Two Photons," CDF Note 1472, June 14, 1991; R. Harris, "Calibration of CPR Conversion Probability from Fully Reconstructed η and π^0 mesons," CDF Note 2318, in preparation.

[23] J. Hauser, D. Joyce and T. Müller, "Pulse Height Response of Fine Mesh Phototubes," CDF Note 2010, March 24, 1993.

[24] J. Strait, "Design Considerations for a Preshower Detector for the CDF End Plugs," CDF Note 2097, June 1, 1993.

[25] S. Kuhlmann, private communication.

[26] P. de Barbaro, presented at the Plug Upgrade Teleconference, February 3, 1994, (February 4, 1994, in Japan).

[27] J. Strait, "Preshower Tile Light Measurements," presented at the Plug Upgrade Teleconference, February 3, 1994, (February 4, 1994, in Japan).

[28] G. Apollinari and A. Titov, "Plug Upgrade Shower Maximum Detector Scintillator and WLS Fiber Choice," CDF Note 2285, October 1, 1993.

[29] R. Bossert, private communication.

[30] Hamamatsu Photononics Corporation data sheets for MCPMTs H4139 and H5828.

[31] This is the average of the measured QE at 520 nm for 10 R4125 PMTs that were purchased as part of the evaluation of tubes for the Plug Upgrade.

[32] Hamamatsu Photononics Corporation data sheet for tube type H4139G-20MOD, serial number ZH2136.

[33] T. Takebayashi, "Preshower Counter R&D," presented at the Plug Upgrade Teleconference, November 11, 1993, (November 12, 1993, in Japan).

[34] J. Hauser, et al., "Plug Shower Maximum Detector - Design Proposal," Version 4, March 12, 1993, Chapter 4 of "CDF Plug Upgrade Conceptual Design Report."

[35] J. Marrafino, et al., "Massless Gaps for Solenoid+Calorimeter," FERMILAB-TM-1766 (1991).

[36] F. Abe, et al., "Pseudorapidity Distributions of charged particles produced in $\bar{p}p$ Interactions at $\sqrt{s}$=630 and 1800 GeV," *Phys. Rev.* *D*41, 2330 (1990).

[37] L. Breccia, et al., Chapter 6 of "CDF Plug Upgrade Conceptual Design Report."